# Master's Thesis

**Master Degree in Energy Engineering**

## Title

# Interactions analysis between VSC converters and an onshore AC Network


**Author:** Rosell Kuen Collart Louie

**Supervisors:** Eduardo Prieto & Luis Orellana


**Date:** September 2019



Escola Tècnica Superior
d'Enginyeria Industrial de Barcelona


## Abstract

This thesis starts by addressing two modelling techniques for power systems in $qd0$-domain. The first technique is the state-space representation, which describes the behaviour of a physical system by means of its state variables in the time domain. The second modelling technique is the admittance matrix, which expresses the voltage-current relationship of the system as a transfer function in the frequency $s$-domain.

The main reason for using these two techniques is because both are equivalent, allows to model the same system in two different ways providing different insights. This is an important point because every modelling technique has its own drawbacks and benefits in terms of derivation and information that they can provide. Deriving properly the model is crucial for studying the behaviour of the system under any condition of operation.

The power network studied in this thesis is comprised by seven overhead power lines interconnecting five buses, this power network is addressed by the name of " Five Bus Network". The state-space model and admittance matrix model of the five Bus network is derived and compared on the basis of eigenvalues and singular values.

Later, a voltage source converter (VSC) is connected to the power system. The power system in this thesis is comprised by a grid-connected VSC converter, an equivalent network and the five bus network. The control system of the VSC converter is described and properly validated to ensure its correct operation.

The two main studied interactions between the VSC converter and the power network are related to the strength of the equivalent network and the disconnection of a power transmission line. The strength of an AC grid is normally defined by the short circuit ratio (SCR), which has negative effects on the stability of the control system of the converter. Also, the loss of a power line imposes new constraints on the system and changes drastically the topology of the network.

The simulations are performed in MATLAB-SIMULINK. Two models are created to capture the dynamics of the system. The first is a non-linear model created in SIMULINK (VSC converter and the AC grid) and the second is a linear model (VSC converter and the AC grid) based on the state space representation. The linear model is validated to assure that matches the non-linear model whenever a small perturbation in the system occurs. Results are expressed in time-domain and in the frequency $s$-domain.

Finally, the obtained results shows the impact of low SCRs on the stability of the system. The lower the SCR, the more prone the system is to become unstable. On the other hand, the loss of a power line limits the power transfer capabilities between the converter and the network. And if proper power adjustments are not made the system could become unstable.

## Acknowledgements

I would like to thank my supervisor Luis Orellana who is currently pursuing his PhD at CITCEA-UPC, for his patience, guidance and help during the course of the project. Thank you very much for your time dedicated to address doubts and questions.

I want to thank my supervisor Prof. Eduardo Prieto, for his support and guidance during the project. His passion for power electronics has spread to me.

Also, I would like to thank Carlos Collados who is currently pursuing his PhD at CITCEA-UPC, for his help and explanations on the reference selection for the PLL.

Special thanks to the CITCEA-UPC research group for their friendship and for providing me of a physical space to develop the thesis.

Special thanks to my friends in Barcelona for their support and friendship.

Finally, I want to thank my friends and family at Honduras for their love and support during these two years of my master degree away from home.

Rosell Collart
Barcelona, Spain
September, 2019

# Contents

# List of Figures

# List of Tables

# 1 Introduction

## 1.1 Scope

The main scope of this thesis is to asses and study the interactions of a grid-connected VSC converter with a meshed AC system. The main interactions studied in this thesis are related to the variation of the short circuit ratio of the equivalent network and the disconnection of a power transmission line in the network.The disconnection could be driven by a fault or a grid operator decision. Normally, the literature studies a simplified model of a power system which is comprised by a VSC converter and an equivalent network. This thesis goes beyond this simplification and seeks to study a more complex and larger power system, one that is formed by five buses and seven overhead power lines. As it will be shown in Section 6, larger power networks introduce some dynamics that are not perceived in simplified systems.

Since the topology of the power system is complex, it is important to derive a proper model of such system. In the literature, power systems are normally modelled in terms of its states variables applying the state-space representation [2]. Another modelling technique is the admittance matrix [3]. This two modelling techniques are detailed and addressed in Section 2. Moreover, in Section 3, the model of the power network is derived applying both modelling techniques in the $qd0$-domain and compared to demonstrate that both techniques are equivalent and lead to the same results.

The proper understanding of these modelling techniques is really important and relevant for this thesis, because a model that is incorrect would not provide accurate results. And the behaviour of the system would not be assessed correctly. Once that the model of the power network is obtained, the VSC converter can be connected. The VSC converter has its respective model of the control system so it can be integrated with the power system model.

The VSC converter model is given in state-space representation, therefore, the model of the complete power system (VSC converter, five bus network and equivalent network) is described by means of the state-space representation. Perhaps, it is not required to derive two modelling techniques if only one is applied. Well, for this thesis having two modelling techniques that are equivalent ensures the exactitude and accuracy of the derived models. Also, one technique might be more convenient than the other in terms of simplicity.

The model of the power system, which is linear because it is written in the state-space representation is compared and validated with a non-linear model built with MATLAB-SIMULINK. For the validation procedure a step in the outer control loop is introduced to cause a small perturbation in the system and capture the dynamic of both models.

With the system properly validated, the short circuit ratio can be varied in order to study the behaviour of the system under different grid strength conditions. The results obtained from these simulations are clear and demonstrates the impact of low short circuit ratio values on the stability of the system. Some control loops are impacted as well, specially the PLL due to the voltage variation.

Similarly, the loss of a power line or a power line outage imposes power transfer limits on the system. The power transfer capabilities of the VSC converter are reduced, if power set-points

are not adjusted the system becomes unstable as the results clearly indicate in Section 7.

The stability of the electrical power system is fundamental for the proper operation of the system. If stability is not addressed properly the system becomes unreliable, inefficient and lastly it impacts on the economy of a society.

This thesis tries to address all the discussed topics in a simple and understandable manner and making the content easy to follow.

## 1.2 Background

The development of high voltage direct current (HVDC) power transmission has brought many advantages over high voltage alternate current (HVAC) power transmission and a set of new possibilities [4]. With the high energy consumption of current societies actual electricity generation projects are challenged to generate and transport major amounts of energy. With the increasing construction of offshore wind power plants, the power transmission distance has become a challenge for energy transmission in a feasible, reliable and efficient way.

HVDC becomes the only solution for undersea power transmission above 50 km, because the charging current above this distance for AC power lines is high and increases the reactive power compensation for power transmission [5]. The HVDC power transmission is achieved by means of a converter station that transforms the alternate current (AC) in direct current (DC) which later is transmitted through HVDC power lines. Two technologies of converter/inverter stations have been set as the standard for HVDC applications, the first technology is the Line Commuted Converter (LCC) which relies on Thyristor valves [4]. LCC it is a proven and well developed technology for high power applications. The second technology is the VSC converter which relies on Isolated gate bipolar transistor (IGBT) valves. VSCs have demonstrated significant advantages over LCC, like independent active and reactive power control, black start capabilities, grid forming mode, lower harmonic content and a considered reduced space for the physical installation of the converter [4]. The majority of HVDC applications take place in remote areas or far away from the main AC grid, therefore, they are normally connected to the main grid by means of long AC power transmission lines. With long distances come an increasing impedance of the line which reduces the short circuit capacity (SCC) of the line.

The short circuit capacity which is measured in MVA is the short circuit power that a power transmission system or line can withstand in the presence of a short circuit. And it is given by the following expression [6]:

$$SCC = \frac{E_{ac}^2}{Z_{th}} \text{ [MVA]}$$

Where $E_{ac}$ is the point of common coupling (PCC) voltage and the $Z_{th}$ is the Thevenin equivalent impedance of the AC system.

The SCC can be related with the DC power $P_{DC}$ that a HVDC converter can exchange with the AC grid to measure the strength of the grid, this new parameter that relates the SCC and the $P_{DC}$ is called the short circuit ratio and is given by the following expression [7]:

$$SCR = \frac{SCC}{P_{DC}} \left[\frac{\text{MVA}}{\text{MW}}\right]$$

LCC converters present instability problems when connected to weak AC grids due to the reactive power compensation required by the converter which makes economically and technically unfeasible to operate under a weak AC grid [8]. There are specific values of SCRs for LCC converters which define when a grid is strong or weak. In [7] the strength of the grid it has been defined as follows:

1. A high SCR AC/DC system is categorized by a SCR value greater than 3.

2. A low SCR AC/DC system is categorized by a SCR value between 2 and 3.

3. A very low SCR AC/DC system is categorized by a SCR value lower than 2.

It was believed that VSC converters would not present any problem related to the strength of the grid because of its control techniques (vector current control). Although, some papers have identified some problems when working under weak and very weak AC grids.

Many authors have attempted to provide a range of SCRs under which an AC grid connected to a VSC converter can be considered strong or weak. In [9], the authors state that the boundary between strong and weak grids is in the range of 1.3 to 1.6 under certain considerations regarding the gains of the PLL. Although, many authors consider grid strength ranges for a VSC converter to be the same as for a LCC converter.

There is literature that encountered problems with the operation of VSC converter connected to weak AC grid, most of them are related to instability problems of certain control loops. The following list provides a brief description of the studies performed:

1. In [10] the resonance stability of the impedance of a VSC-HVDC system is analyzed. The main impacting factors on stability are the feedforward filter of the current control loop, the line length and the power transfer levels.

2. In [9] a small signal stability analysis is applied to investigate how the power system impedance and the parameters of the PLL influence the dynamic behavior and the stability limits of the VSC in HVDC applications.

3. In [11] the viability of vector control in an extremely weak grid (SCR=1) is studied, important instabilities are addressed in the outer control loop of the converter when dealing with high-power demands.

4. In [12] the stability impact of the open loop AC voltage control of a weak grid connected DFIG is studied through a small signal transfer function model. The high gains of the AC voltage controller impose power transfer and stability limits. However, the authors did not propose any solution to improve the stability limits of the AC voltage control.

5. In [13] a power compensation control it is proposed to achieve two objectives : First, to restrain the response of the active power so there is more time left to the AC voltage controller to generate corresponding reactive power. Second, to enhance the response of the AC voltage loop to suppress the PCC voltage fluctuation. An active damping filter has been proposed for the inner loop control to suppress the resonance created by the capacitor in the PCC.

6. In [14] a small signal analysis of the DC voltage controller of a VSC converter is proposed to determine the stability of the controller connected to a weak grid. The stability of the DC voltage controller it is worsen when the strength of the system diminishes or when the power level is increased when connected a weak grid. Moreover, important interactions of the control loops are identified. PLL bandwidth has a direct effect on the DC voltage controller. No solution provided to mitigate the effects of low SCR.

7. In [15] a frequency based synchronization control is proposed to provide damping for the oscillations created by the PLL when connected to a weak AC grid.

8. In [16] two solutions are proposed for a VSC converter connected to a weak AC grid. The first solution comprises a tuning of the PLL and AC voltage controller gains, and the second solution, considers the creation of an artificial bus for the grid-connected converter to reduce the effective grid impedance viewed by the VSC.

9. In [17] a power synchronization control (PSC) is proposed to overcome the drawbacks of the vector-current control due to low SCRs. The power synchronization control is based on the power synchronization principal of synchronous machines (SMs), therefore, the VSC behaves as a SM providing strong voltage support. Moreover, it has no requirement on the short circuit capacity of the AC system.

The literature reviewed also provides some proposals or solutions to address the weak AC grids phenomenon, some papers only point out the problems generated in the VSC converter near a weak grid and others identify the problem and propose a solution to mitigate the negative effects of high impedance grids.

1. In [9] and [14] the effect of the PLL parameters on the VSC converter are identified and studied, although, there is not any solution provided to mitigate the effect of the PLL. Although, in [9] it is pointed out that at a $K_p > 60$ and at a SCR = 1.3 the VSC becomes unstable. Therefore, small gain values would become the system stable but this would provide a small damping and poor dynamic performance at higher SCRs.

2. In [11] and [13] a new outer control loop is proposed. In [11] an advanced vector control is proposed to mitigate the effects of the weak grid on the outer control loop. The new outer control loop has 35 robust local controllers, but, such controllers require a high tuning complexity. In [13] the power compensation control seeks to compensate the active and reactive power by means of enhanced controllers for the active power and AC voltage control loops of the traditional vector-current control method. The main goal of the power compensation control is to reduce the response of the active power and increase the response of AC voltage control loop for improving the generation of reactive power restraining the fluctuations of the PCC voltage, therefore, improving stability of the system.

3. In [16] the PLL is identified as the main source of instability, therefore, tuning the PLL and the voltage regulator parameters together is proposed. By doing the tuning procedure together, it is achieved a very slow PLL and a very fast voltage regulator so their interactions do not make the system unstable. However, there is not a detailed procedure on how to tune the controllers in the paper and some drawbacks are encountered with the retuned controllers.

4. In [10] no solutions were provided to the listed instability factors of the VSC converter connected to a high impedance grid. Although, it provides a thorough study of the electrical resonances present in the impedance of the VSC converter due to the feedforward filter, line inductance and level of power transfer.

5. More than an improvement, the PSC [17] is a new control method to deal with low SCR grids. The PSC eliminates the necessity of the PLL, therefore, the VSC is able to work stable under weak grids. Although, one of the best features of vector current control is the ability to limit the currents under fault conditions and this feature is lost in the PSC making the converter to switch to the traditional vector current control and to have a backup PLL to deal with fault conditions.

As it can be seen, weak AC grids is an interesting and relevant topic that has been the focus of many studies. In this thesis it will be studied and assessed its impact on the stability of a system.

## 1.3 Structure of the thesis

The thesis is organized into seven sections. In **Section 1** the scope, background information and structure of the thesis is detailed. In **Section 2** the theoretical framework for the modelling techniques for power networks is developed and explained. **Section 3** goes in depth an introduces the application of the modelling techniques, firstly by applying them to simple passive elements of the network and then it builds up to the more complex power network topologies. **Section 4** provides the mathematical tools to compare the modelling techniques applied later in the thesis to assess the results. There is also a graphic comparison of the five bus network applying the mentioned mathematical tools. **Section 5** list the characteristics and parameters of the studied power system in this thesis. **Section 6** introduces the control system of the VSC converter. Also, it is detailed the linear model of the control system. Validation of the non-linear and linear model is detailed and performed by dynamic simulations in time. Finally, **Section 7** details the studied interactions and provides the results.

## 1.4 Computational tools

The use of programs for developing projects like this is indispensable and necessary, they provide useful tools that reduce the complexity of many procedures.

The development of many of the equation systems derived during the course of the project were performed by using the Maple software [18]. Maple is a powerful mathematical software for solving mathematical problems of any kind. It provides an interactive and user friendly interface easy to use and also has a detailed user manual that helps to address any doubt or problem with the software itself. Maple software was used mostly in the development of Section 4, this section is rich in mathematical content.

The second software utilized extensively in this project is MATLAB-SIMULINK. Equations derived in Maple were introduced in MATLAB for simulations purposes and extraction of results. Non-linear and linear dynamic models were built in SIMULINK for Sections 6 and 7.

# 2 Theoretical framework

In this section, it is introduced the theoretical framework for the modelling techniques applied in this thesis. First, it is described and explained the admittance matrix. Second, the state-space representation of a system is detailed. Moreover, a mathematical comparison is performed for both modelling techniques to show its equivalence. Finally, the mathematical background for the $qd0$-domain is addressed.

It is important to clarify that these topics are addressed in a general way. For more detailed information the reader is referred to the references or external information. In this section no examples are given.

## 2.1 Admittance matrix

A power system network can be modelled as an equivalent admittance analysis purposes. This matrix form the basis of power flow and short circuit studies. In this section it is discussed the construction of the admittance matrix, which is used extensively in this thesis.

### 2.1.1 Admittance matrix construction

Applying Kirchhoff's voltage law to the circuit of Fig. 1a, which is formed by a voltage source $\underline{E}_s$ connected in series with an impedance $\underline{Z}_s$ and has a voltage $V$ at the terminals, then:

$$\underline{E}_s = \underline{Z}_s \underline{I} + \underline{V} \tag{2.1}$$

Dividing (2.1) by $\underline{Z}_s$, it is obtained the current equation for Fig. 1b:

$$\underline{I}_s = \frac{\underline{E}_s}{\underline{Z}_s} = \underline{I} + \underline{Y}_s \underline{V} \tag{2.2}$$

where $\underline{Y}_s = 1/\underline{Z}_s$. Therefore, the voltage source $\underline{E}_s$ with its series impedance $\underline{Z}_s$ can be exchanged by a current source $\underline{I}_s$ with its parallel admittance $\underline{Y}_s$. The sources $\underline{E}_s$ and $\underline{I}_s$ are connected externally to the nodes or buses of the transmission networks, which are basically formed by passive branches (power lines). Therefore, power lines can be represented by its branch impedance $\underline{Z}_s$ or branch admittance $\underline{Y}_s$.

The equations for the current-voltage relationship of a power line are:

$$\underline{V}_a = \underline{Z}_s \underline{I}_a \quad \text{or} \quad \underline{Y}_s \underline{V}_a = \underline{I}_a \tag{2.3}$$

where $\underline{V}_a$ is the voltage drop through the power line in the direction of the current $\underline{I}_a$. The typical power lines has two variables associated $\underline{V}_a$ and $\underline{I}_a$, independently on how is connected the power line to the network.

In order to explain the method properly, consider Fig. 2, where a power line of admittance $\underline{Y}_s$ is connected between two nodes or buses 1 and 2. Assume that this power line is part of a big network. The currents $\underline{I}_1$ and $\underline{I}_2$ are considered positives, because it is assumed they are

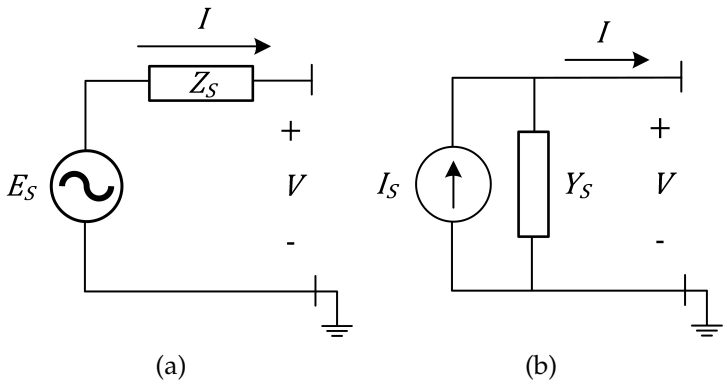


(a) (b)

Figure 1: Equivalent circuits

injected into the network. The currents that leave the network at any bus are considered as negatives. For example, when a load is connected to the network at any bus the current that feeds the load is considered negative because leaves the network. Voltages $\underline{V}_1$ and $\underline{V}_2$ are the voltages

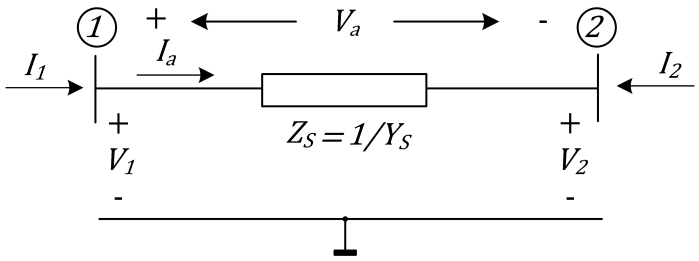


Figure 2: Power line

measured at bus 1 and bus 2 respect to ground or the reference node.

Applying Kirchhoff's current law at every bus, the following relationships are obtained:

$$\begin{bmatrix} \underline{I}_1 \\ \underline{I}_2 \end{bmatrix} = \begin{bmatrix} 1 \\ -1 \end{bmatrix} \underline{I}_a \tag{2.4}$$

Likewise, the voltage drop $\underline{V}_a$ can be obtained:

$$\underline{V}_a = [1 \quad -1] \begin{bmatrix} \underline{V}_1 \\ \underline{V}_2 \end{bmatrix} \tag{2.5}$$

Substituting (2.5) in $\underline{Y}_s \underline{V}_a = \underline{I}_a$, it is obtained:

$$\underline{Y}_s [1 \quad -1] \begin{bmatrix} \underline{V}_1 \\ \underline{V}_2 \end{bmatrix} = \underline{I}_a \tag{2.6}$$

And if every side of (2.6) is multiplied by the column vector of (2.4), then:

$$\begin{bmatrix} 1 \\ -1 \end{bmatrix} \underline{Y}_s [1 \quad -1] \begin{bmatrix} \underline{V}_1 \\ V_2 \end{bmatrix} = \begin{bmatrix} \underline{I}_1 \\ \underline{I}_2 \end{bmatrix} \tag{2.7}$$

Simplifying (2.7):

$$\begin{bmatrix} \underline{Y}_s & -\underline{Y}_s \\ -\underline{Y}_s & \underline{Y}_s \end{bmatrix} \begin{bmatrix} \underline{V}_1 \\ \underline{V}_2 \end{bmatrix} = \begin{bmatrix} \underline{I}_1 \\ \underline{I}_2 \end{bmatrix} \tag{2.8}$$

The coefficient matrix of (2.8) is the admittance matrix $Y_{mat}$ of the power line of Fig. 2. The off-diagonal elements of the matrix are always negative and for this case are equal to the diagonal elements. The derivation of the equations for the admittance matrix are taken from [3].

### 2.1.2 Connecting a voltage source

If a voltage source $\underline{V}_g$ with an impedance $\underline{Z}_g$ is connected to the bus 1, the admittance matrix would need to be calculated all over again because the system is different now. One of the advantages of the admittance matrix, is that it is really easy to be modified. In order to be modified, the impedance $\underline{Z}_g$ needs to be inverted to obtain the admittance $\underline{Y}_g$ and the voltage source becomes a current source $\underline{I}_g$. Where $\underline{I}_g = \underline{Y}_g \underline{V}_g$. Since the admittance $\underline{Y}_g$ is connected to bus 1, this will be summed with the first element of the admittance matrix of (2.8) and the current $\underline{I}_1$ becomes $\underline{I}_g$.

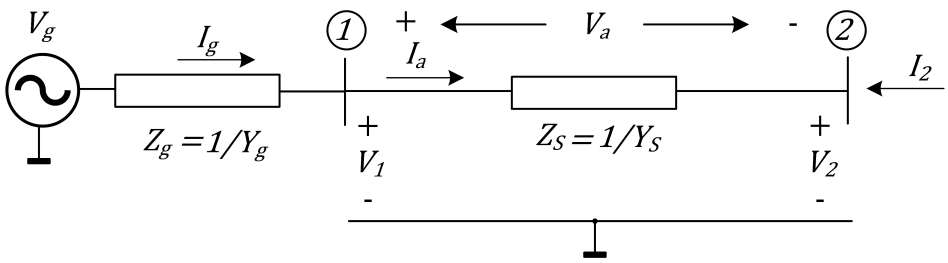


Figure 3: Power RL line plus voltage source

Making the proper substitutions in (2.8), it becomes:

$$\begin{bmatrix} \underline{Y}_s + \underline{Y}_g & -\underline{Y}_s \\ -\underline{Y}_s & \underline{Y}_s \end{bmatrix} \begin{bmatrix} \underline{V}_1 \\ \underline{V}_2 \end{bmatrix} = \begin{bmatrix} \underline{I}_g \\ \underline{I}_2 \end{bmatrix} \tag{2.9}$$

### 2.1.3 Pi line model

If the power line of admittance $\underline{Y}_s$ used previously is changed by a pi line model, the admittance matrix of (2.8) needs to be redefined for the new changes. Fig. 4 depicts the pi line:
Note that $\underline{Y}_s$ has been changed for $\underline{Y}_L$, this is just to differentiate the elements of the pi line. Where $\underline{Y}_L$ corresponds to the series inductor resistor admittance and $\underline{Y}_C$ corresponds to the shunt capacitor admittances.

Every element $Y_{nn}$ of the diagonal in the admittance matrix is the sum of all admittances connected to the bus or node "$n$". The off-diagonal elements remain the same, they only consider the admittance element that relates two buses connected by that power line series admittance.

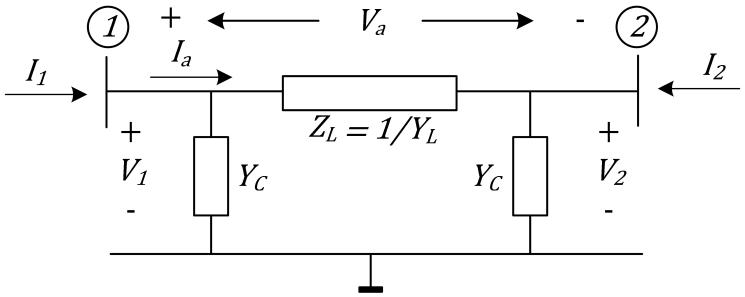


Figure 4: Pi power line

Therefore, the current-voltage relationship for the admittance matrix of the pi lines is as follows:

$$\begin{bmatrix} \underline{Y}_L + \underline{Y}_C & -\underline{Y}_L \\ -\underline{Y}_L & \underline{Y}_L + \underline{Y}_C \end{bmatrix} \begin{bmatrix} \underline{V}_1 \\ \underline{V}_2 \end{bmatrix} = \begin{bmatrix} \underline{I}_1 \\ \underline{I}_2 \end{bmatrix} \tag{2.10}$$

And if a voltage source $\underline{V}_g$ with an impedance $\underline{Z}_g$ is connected to bus 1, the current-voltage relationship for the admittance matrix is:

$$\begin{bmatrix} \underline{Y}_L + \underline{Y}_C + \underline{Y}_g & -\underline{Y}_L \\ -\underline{Y}_L & \underline{Y}_L + \underline{Y}_C \end{bmatrix} \begin{bmatrix} \underline{V}_1 \\ \underline{V}_2 \end{bmatrix} = \begin{bmatrix} \underline{I}_g \\ \underline{I}_2 \end{bmatrix} \tag{2.11}$$

As it has been shown, the construction of the admittance matrix is easy and straightforward making it suitable for power network studies. Its simplicity allows to check for possible mistakes during the construction process. Also, there are algorithms to obtain the admittance matrix using computational tools, these algorithms are not discussed in this thesis because they are out of the scope.

For further discussions regarding the admittance matrix, it is going to be expressed in compact form as follows:

$$\mathbf{Y_{mat}} \mathbf{V_{mat}} = \mathbf{i_{mat}} \tag{2.12}$$

Where, $Y_{mat}$ is the admittance matrix, $i_{mat}$ are the input currents of the network and $V_{mat}$ the voltages at every bus. The subscript "$mat$" stands for $matrix$. In this thesis, variables in bold letters are used to represent matrices in compact form.

## 2.2 State-space representation

The state-space (SS) representation is a mathematical tool that allows to analyze and understand complex linear time-invariant systems. It is a tool used in many disciplines, being electrical engineering one among them [19]. An electrical network can be modelled by a set of first-order differential equations, which describe the dynamic behavior of the network.

In the state-space representation a collection of variables are specified to describe the internal behavior of the system. These variables are known as the state variables of the system. By definition: a **state variable** is a physical property that characterizes the state of a system, regardless of how the system got to that state [19].

In an electric circuit, the state variables are the inductor current $i_L$ and capacitor voltage $v_L$ since they collectively describe the energy state of the system.

$$v_L = L\frac{d}{dt}i_L \quad \text{and} \quad i_c = C\frac{d}{dt}v_c \tag{2.13}$$

The state-space representation is formed by the following set of equations:

$$\dot{\mathbf{x}}(t) = \mathbf{A}\mathbf{x}(t) + \mathbf{B}\mathbf{u}(t) \quad \mathbf{y}(t) = \mathbf{C}\mathbf{x}(t) + \mathbf{D}\mathbf{u}(t) \tag{2.14}$$

Where $\mathbf{x}(t)$ is the state vector formed by state variables and the dot in $\dot{\mathbf{x}}(t)$ represents the first derivative with respect to time, $\mathbf{u}(t)$ are the excitation functions of the system or input vector. Normally the desired outputs may or may not be the state variables, therefore, the desired outputs must be expressed in terms of $\mathbf{x}(t)$ and $u(t)$ to form the output vector $\mathbf{y}(t)$ of the system. In matrix form $\mathbf{x}(t)$, $\mathbf{u}(t)$ and $\mathbf{y}(t)$ are :

$$\mathbf{x}(t) = \begin{bmatrix} x_1(t) \\ x_2(t) \\ \vdots \\ x_n(t) \end{bmatrix} \quad \mathbf{u}(t) = \begin{bmatrix} u_1(t) \\ u_2(t) \\ \vdots \\ u_m(t) \end{bmatrix} \quad \mathbf{y}(t) = \begin{bmatrix} y_1(t) \\ y_2(t) \\ \vdots \\ y_p(t) \end{bmatrix} \tag{2.15}$$

The coefficients **A** and **B** are respectively $n \times n$ and $n \times m$ matrices, the coefficients **C** and **D** are respectively $p \times n$ and $p \times m$ matrices.

This is a short and brief description of the state-space representation topic, however, the literature is vast and extensive. In this thesis, it is only introduced an overall explanation regarding the subject.

In Section 3, there are many examples developed applying the SS representation to model different power networks, therefore, no examples are given in this section.

## 2.3 Admittance matrix in the $s$-domain

In electrical engineering the terms impedance or admittance are commonly used to describe the algebraic current-voltage relationship in electrical elements, which is primarily based on the Ohm's law. The admittance matrix (AM) is developed in this thesis in terms of transfer functions.

A **transfer function** is the ratio $H(s)$ of the Laplace transform of the output function $y(t)$, to the Laplace transform of the input $u(t)$, assuming that there is only one input [14]. A transfer function $H(s)$ is given by the following expression:

$$H(s) = \frac{Y(s)}{U(s)} = \frac{\text{output}}{\text{input}} \tag{2.16}$$

It can be seen that the transfer function $H(s)$ is function of the complex frequency $s$, where $s = j\omega$.

In Section 2.1, it was introduced the concept of admittance matrix. Notice that (2.12) resembles the form of a transfer function, because it relates the input currents with the output voltages.

Arranging (2.12) properly, then:

$$\mathbf{H^{AM}}(s) = \frac{\mathbf{V_{mat}}(s)}{\mathbf{i_{mat}}(s)} = \frac{\mathbf{V_{mat}}(s)}{\mathbf{Y_{mat}}(s)\mathbf{V_{mat}}(s)} = \frac{1}{\mathbf{Y_{mat}}(s)} = \mathbf{Z_{mat}}(s) \tag{2.17}$$

Notice that it is not the admittance matrix itself the relevant one but the impedance matrix, as it is shown in (2.17). However, the $Y_{mat}$ allows to obtain easily the $Z_{mat}$ just by performing an algebraic operation [20]. Altogether, the interest relies on the $H^{AM}(s)$ term and not on the possible output response due to certain input. Moreover, the $H^{AM}(s)$ term contains the entire information of the network, which is essential for dynamic studies. More of this in Section 4.

Lastly, it is important to note that the inversion procedure can become a challenging task when the order of the matrix increases considerably. By order of the matrix, it means to have a very large power network. Because every element of the matrix is a transfer function of a high degree polynomial in the numerator and denominator. Alternative procedures for inverting the matrix should be used or the impedance matrix should be obtained directly through proper algorithms.

### 2.3.1 Relation between admittance matrix and state-space representation

The SS representation can be transformed into a transfer function if proper mathematical procedures are applied [19]. The importance of relating both modelling techniques is to demonstrate they are equivalent and this allows to compare and analyze the behaviour of a certain system, in this case, a power network. The mathematical tools to compare both systems are not described in this section, but they are in Section 4.

Applying the Laplace transform to (2.14) for the SS representation, then:

$$\begin{aligned} s\mathbf{X}(s) &= \mathbf{A}\mathbf{X}(s) + \mathbf{B}\mathbf{U}(s) \\ \mathbf{Y}(s) &= \mathbf{C}\mathbf{X}(s) + \mathbf{D}\mathbf{U}(s) \end{aligned} \tag{2.18}$$

All initial conditions are considered to be zero.

Solving for $X(s)$ and substituting it in $Y(s)$ in (2.18):

$$\begin{aligned} \mathbf{X}(s) &= (s\mathbf{I} - \mathbf{A})^{-1}\mathbf{B}\mathbf{U}(s) \\ \mathbf{Y}(s) &= \mathbf{C}(s\mathbf{I} - \mathbf{A})^{-1}\mathbf{B}\mathbf{U}(s) + \mathbf{D} + \mathbf{U}(s) \end{aligned} \tag{2.19}$$

If the expression obtained in (2.19) for $Y(s)$ is arranged as a transfer function, then substituting it in (2.16) and considering that the input of the system is $U(s)$. The $D$ coefficient is zero, then:

$$\mathbf{H^{SS}}(s) = \frac{\mathbf{C}(s\mathbf{I} - \mathbf{A})^{-1}\mathbf{B}\mathbf{U}(s)}{\mathbf{U}(s)} = \mathbf{C}(s\mathbf{I} - \mathbf{A})^{-1}\mathbf{B} \tag{2.20}$$

To clarify, the D coefficient is zero because the chosen outputs are only dependent on the state variables, this means that the outputs are indeed the state variables of the system. It has been demonstrated in (2.20), that the state-space representation can be transformed into a transfer function. This becomes really helpful when modelling the system with the admittance matrix becomes challenging.

In Section 3, there are some examples developed applying the AM to model different power networks, therefore, no examples are given in this section.

## 2.4 dq0 domain

This section addresses the mathematical formulation behind the qd0 domain. On previous sections it was introduced the state-space representation and the admittance matrix as techniques to model a power network. These modelling techniques are coupled with the $qd0$-domain, as it is going to be shown in Section 3. This means that the state-space representation and admittance matrix are model in the time-qd domain and the complex frequency-qd domain, respectively.

The $dq0$ domain departs from the instantaneous power theory that introduces the Clarke transformation matrix [21]. This transformation allows to transform sinusoidal three-phase signals (120° phase-shift between phases) into two sinusoidal signals (90° phase-shift between phases).

$$\left[\mathbf{X}_{\alpha\beta 0}\right] = \left[T_{\alpha\beta 0}\right]\left[\mathbf{X}_{abc}\right] \tag{2.21}$$

The third signal in the $\alpha\beta 0$ domain is the zero sequence component. If the three-phase system in the $abc$ domain is without neutral, therefore, in the $\alpha\beta 0$ domain the vector in (2.21) is only defined by two signals.

Where $T_{\alpha\beta 0}$ [21] is:

$$T_{\alpha\beta 0} = \frac{2}{3}\begin{bmatrix} 1 & -\frac{1}{2} & -\frac{1}{2} \\ 0 & -\frac{\sqrt{3}}{2} & \frac{\sqrt{3}}{2} \\ \frac{1}{2} & \frac{1}{2} & \frac{1}{2} \end{bmatrix} \tag{2.22}$$

The $\alpha\beta 0$ domain is useful for many applications, although, it still has the oscillatory characteristics of the $abc$ domain [22]. For control purposes, it is better to work with constant quantities, this is where the Park transformation is introduced. This transformation allows to transform two sinusoidal signals (90° phase-shift between phases) into two constant quantities. To do so, a rotation is performed to (2.21), and is given by the following matrix:

$$R\left(\theta\right) = \begin{bmatrix} \cos\left(\theta\right) & -\sin\left(\theta\right) & 0 \\ \sin\left(\theta\right) & \cos\left(\theta\right) & 0 \\ 0 & 0 & 1 \end{bmatrix} \tag{2.23}$$

Applying the rotation matrix to (2.22), the Park transformation matrix is:

$$T(\theta) = \left[R\left(\theta\right)\right]\left[T_{\alpha\beta 0}\right] = \frac{2}{3}\begin{bmatrix} \cos\left(\theta\right) & \cos\left(\theta - \frac{2\pi}{3}\right) & \cos\left(\theta + \frac{2\pi}{3}\right) \\ \sin\left(\theta\right) & \sin\left(\theta - \frac{2\pi}{3}\right) & \sin\left(\theta + \frac{2\pi}{3}\right) \\ \frac{1}{2} & \frac{1}{2} & \frac{1}{2} \end{bmatrix} \tag{2.24}$$

$$\left[\mathbf{X}_{qd0}\right] = \left[T(\theta)\right]\left[\mathbf{X}_{abc}\right] \tag{2.25}$$

It is useful to get the inverse of the Park transformation matrix, then:

$$T(\theta)^{-1} = \begin{bmatrix} \cos\left(\theta\right) & \sin\left(\theta\right) & 1 \\ \cos\left(\theta - \frac{2\pi}{3}\right) & \sin\left(\theta - \frac{2\pi}{3}\right) & 1 \\ \cos\left(\theta + \frac{2\pi}{3}\right) & \sin\left(\theta + \frac{2\pi}{3}\right) & 1 \end{bmatrix} \tag{2.26}$$

# 3 Power network modelling

This section comprises the mathematical formulation in $qd0$-domain of the passive elements that forms a power network. These passive elements are the resistor, inductor and capacitor. Also, the modeling techniques introduced in Section 2 are applied and developed for a set of network topologies. The development of the content described in this section goes from the simplest elements to the most complex network topologies.

Once the passive elements and the different network topologies are described, the concept of equivalent network is introduced and developed.

## 3.1 Inductive element

### 3.1.1 State-space model

In this section, the development of the current-voltage relationship for an inductive element in time-qd domain is developed. Fig. 5 depicts a series inductor resistor with $L$ and $R$ constants, respectively.

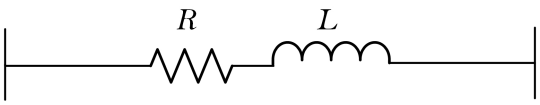


Figure 5: Series inductor resistor

The current-voltage relationship for an inductor is given by the following expression:

$$\begin{bmatrix} V_{La} \\ V_{Lb} \\ V_{Lc} \end{bmatrix} = \begin{bmatrix} L & 0 & 0 \\ 0 & L & 0 \\ 0 & 0 & L \end{bmatrix} \frac{d}{dt} \begin{bmatrix} i_{La} \\ i_{Lb} \\ i_{Lc} \end{bmatrix} \tag{3.1}$$

Writing (3.1) in compact form :

$$\mathbf{V_{Labc}} = L\mathbf{I_3}\frac{d}{dt}\mathbf{i_{Labc}} \tag{3.2}$$

Where the identity matrix is denoted as $I_n$ and the subscript $n$ denotes the size of the matrix. Transforming (3.2) from the $abc$ domain to $qd0$-domain, applying the transformation matrix $T(\theta)$:

$$T(\theta)\mathbf{V_{Labc}} = T(\theta)L\mathbf{I_3}\frac{d}{dt}\mathbf{i_{Labc}} \tag{3.3}$$

Where:

$$T(\theta)\mathbf{V_{Labc}} = \mathbf{V_{Lqd0}} \tag{3.4}$$

A special consideration needs to be done on the derivative of the current in (3.3). In order to obtain the derivative of the current in $qd0$-domain the following mathematical procedure is

performed. Knowing that:

$$\mathbf{i_{Labc}} = T(\theta)^{-1}\mathbf{i_{Lqd0}} \tag{3.5}$$

Substituting (3.4) and (3.5) in (3.3):

$$\mathbf{V_{Lqd0}} = T(\theta)L\mathbf{I_3}\frac{d}{dt}\left(T(\theta)^{-1}\mathbf{i_{Lqd0}}\right) \tag{3.6}$$

Applying the product rule for derivatives to (3.6):

$$\mathbf{V_{Lqd0}} = T(\theta)L\mathbf{I_3}\left(\mathbf{i_{Lqd0}}\frac{d}{dt}T(\theta)^{-1} + T(\theta)^{-1}\frac{d}{dt}\mathbf{i_{Lqd0}}\right) \tag{3.7}$$

Expanding (3.7):

$$\mathbf{V_{Lqd0}} = T(\theta)L\mathbf{I_3}\mathbf{i_{Lqd0}}\frac{d}{dt}T(\theta)^{-1} + T(\theta)L\mathbf{I_3}T(\theta)^{-1}\frac{d}{dt}\mathbf{i_{Lqd0}} \tag{3.8}$$

From (3.8), the derivative of $T(\theta)^{-1}$ must be determined. Knowing that $\theta = \omega\, t$, the following expression is obtained:

$$\frac{d}{dt}T(\theta)^{-1} = \begin{bmatrix} -\omega\sin(\theta) & \omega\cos(\theta) & 0 \\ -\omega\sin(\theta - 2\pi/3) & \omega\cos(\theta - 2\pi/3) & 0 \\ -\omega\sin(\theta + 2\pi/3) & \omega\cos(\theta + 2\pi/3) & 0 \end{bmatrix} \tag{3.9}$$

To simplify completely (3.8) further mathematical procedures must be done to obtain such equation in $qd0$-domain. As it is shown in the following procedures:

$$\left[T(\theta)L\mathbf{I_3}\mathbf{i_{Lqd0}}\frac{d}{dt}T(\theta)^{-1}\right]\Big|_{\theta=2\pi ft} = \begin{bmatrix} 0 & \omega L & 0 \\ -\omega L & 0 & 0 \\ 0 & 0 & 0 \end{bmatrix}\mathbf{i_{Lqd0}} \tag{3.10}$$

$$\left[T(\theta)L\mathbf{I_3}T(\theta)^{-1}\frac{d}{dt}\mathbf{i_{Lqd0}}\right]\Big|_{\theta=2\pi ft} = \begin{bmatrix} L & 0 & 0 \\ 0 & L & 0 \\ 0 & 0 & 0 \end{bmatrix}\frac{d}{dt}\mathbf{i_{Lqd0}} \tag{3.11}$$

Equations (3.10) and (3.11) are reduced to simpler expressions by evaluating the sines and cosines at the grid angle, at any time $t$ and at the frequency $f(\mathrm{Hz})$ of the grid. Substituting (3.10) and (3.11) in (3.8), it is obtained:

$$\mathbf{V_{Lqd0}} = \begin{bmatrix} 0 & \omega L & 0 \\ -\omega L & 0 & 0 \\ 0 & 0 & 0 \end{bmatrix}\mathbf{i_{Lqd0}} + \begin{bmatrix} L & 0 & 0 \\ 0 & L & 0 \\ 0 & 0 & 0 \end{bmatrix}\frac{d}{dt}\mathbf{i_{Lqd0}} \tag{3.12}$$

Eliminating the homopolar terms of (3.12):

$$\mathbf{V_{Lqd}} = \begin{bmatrix} 0 & \omega L \\ -\omega L & 0 \end{bmatrix} \mathbf{i_{Lqd}} + \begin{bmatrix} L & 0 \\ 0 & L \end{bmatrix} \frac{d}{dt}\mathbf{i_{Lqd}} \tag{3.13}$$

The effect of the transformation matrix has been demonstrated and developed for an inductor. To reduce the mathematical procedures for grid modeling purposes, henceforth, the following mathematical simplification is used for the inductor impedance $\mathbf{Z_L^{SS}}$:

$$\mathbf{Z_L^{SS}} = \begin{bmatrix} L & 0 & 0 & \omega L \\ 0 & L & -\omega L & 0 \end{bmatrix} \tag{3.14}$$

It was shown in (3.7) that the transformation of the derivative term of the current gives two different terms for the current. The first one is $i_{qd}$ and the second one is $\frac{d}{dt}i_{qd}$, ordered in matrix form:

$$\mathbf{I_L^{SS}} = \begin{bmatrix} \mathbf{\frac{d}{dt}i_{Lqd}} & \mathbf{i_{Lqd}} \end{bmatrix}^T = \begin{bmatrix} \frac{d}{dt}i_{Lq} & \frac{d}{dt}i_{Ld} & i_{Lq} & i_{Ld} \end{bmatrix}^T \tag{3.15}$$

Therefore, the current-voltage relationship for the inductor in the time-qd domain can be represented by the following expression:

$$\mathbf{V_L^{SS}} = \mathbf{Z_L^{SS}}\mathbf{I_L^{SS}} \tag{3.16}$$

### 3.1.2 Admittance matrix model

In the previous section the current-voltage relationship for an inductor in time-qd domain was obtained. It is equally important to obtain the current-voltage relationship in frequency-qd domain. The mathematical effect of the transformation matrix was previously demonstrated, which makes the application of the Laplace transform straightforward.

Applying the Laplace transform to (3.12):

$$\mathscr{L}\{\mathbf{V_{Lqd}}\} = \begin{bmatrix} 0 & \omega L \\ -\omega L & 0 \end{bmatrix} \mathscr{L}\{\mathbf{i_{Lqd}}\} + \begin{bmatrix} L & 0 \\ 0 & L \end{bmatrix} \mathscr{L}\left\{\frac{d}{dt}\mathbf{i_{Lqd}}\right\} \tag{3.17}$$

For simplicity, the transformed variables in frequency domain do not appear in the conventional form as $\mathbf{X(s)}$ and they are just simply expressed as $\mathbf{X}$.
All initial conditions are considered to be zero, simplifying and grouping like terms of (3.17):

$$\mathbf{V_{Lqd}} = \begin{bmatrix} Ls & \omega L \\ -\omega L & Ls \end{bmatrix} \mathbf{i_{Lqd}} \tag{3.18}$$

Now it can be defined the impedance of the current-voltage relationship for an inductor in frequency-qd domain:

$$\mathbf{Z_L^{AM}} = \begin{bmatrix} Ls & \omega L \\ -\omega L & Ls \end{bmatrix} \tag{3.19}$$

In general, the inductor is represented with a resistor in series, what is normally called a series inductor resistor. If the resistance is taken into account (3.19) needs to be redefined as follows:

$$\mathbf{Z_L^{AM}} = \begin{bmatrix} Ls+R & \omega L \\ -\omega L & Ls+R \end{bmatrix} \tag{3.20}$$

## 3.2 Capacitive element

### 3.2.1 State-space model

For the capacitor a similar expression can be found when the transformation matrix is applied. Fig. 6 depicts the capacitor $C$:

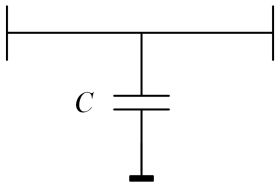


Figure 6: Capacitor

The current-voltage relationship for a capacitor is given by the following expression:

$$\begin{bmatrix} i_{Ca} \\ i_{Cb} \\ i_{Cc} \end{bmatrix} = \begin{bmatrix} C & 0 & 0 \\ 0 & C & 0 \\ 0 & 0 & C \end{bmatrix} \frac{d}{dt} \begin{bmatrix} V_{Ca} \\ V_{Cb} \\ V_{Cc} \end{bmatrix} \tag{3.21}$$

Writing (3.21) in compact form :

$$\mathbf{i_{Cabc}} = C\mathbf{I_3}\frac{d}{dt}\mathbf{V_{Cabc}} \tag{3.22}$$

Applying the transformation matrix $T(\theta)$ to (3.22):

$$\begin{aligned} T(\theta)\,\mathbf{i_{Cabc}} &= T(\theta)C\mathbf{I_3}\frac{d}{dt}\mathbf{V_{Cabc}} \\ \mathbf{i_{Cqd0}} &= T(\theta)C\mathbf{I_3}\left(\mathbf{V_{Cqd0}}\frac{d}{dt}T(\theta)^{-1} + T(\theta)^{-1}\frac{d}{dt}\mathbf{V_{Cqd0}}\right) \end{aligned} \tag{3.23}$$

Simplifying and eliminating the homopolar terms of (3.23):

$$\mathbf{i_{Cqd}} = \begin{bmatrix} 0 & \omega C \\ -\omega C & 0 \end{bmatrix}\mathbf{V_{Cqd}} + \begin{bmatrix} C & 0 \\ 0 & C \end{bmatrix}\frac{d}{dt}\mathbf{V_{Cqd}} \tag{3.24}$$

The effect of the transformation matrix it has been demonstrated and developed for the capacitor. To reduce the mathematical procedures for grid modeling purposes, henceforth, following mathematical simplification is used for the capacitor impedance $\mathbf{Z_C^{SS}}$:

$$\mathbf{Z_C^{SS}} = \begin{bmatrix} C & 0 & 0 & \omega C \\ 0 & C & -\omega C & 0 \end{bmatrix}^{-1} \tag{3.25}$$

It was shown in (3.23) that the transformation of the derivative term of the voltage gives two different terms for the voltage. The first one is $V_{qd}$ and the second one is $\frac{d}{dt}V_{qd}$, ordered in matrix form:

$$\mathbf{V_C^{SS}} = \begin{bmatrix} \mathbf{\frac{d}{dt}V_{Cqd}} & \mathbf{V_{qd}} \end{bmatrix}^T = \begin{bmatrix} \frac{d}{dt}V_{Cq} & \frac{d}{dt}V_{Cd} & V_{Cq} & V_{Cd} \end{bmatrix}^T \tag{3.26}$$

Therefore, the current-voltage relationship for the capacitor in the time-qd domain can be represented by the following expression:

$$\mathbf{i_C^{SS}} = \mathbf{Z_C^{SS\,-1}V_C^{SS}} \tag{3.27}$$

### 3.2.2 Admittance matrix model

Applying the Laplace transform to (3.23) :

$$\mathscr{L}\{\mathbf{i_{Cqd}}\} = \begin{bmatrix} 0 & \omega C \\ -\omega C & 0 \end{bmatrix} \mathscr{L}\{\mathbf{V_{Cqd}}\} + \begin{bmatrix} C & 0 \\ 0 & C \end{bmatrix} \mathscr{L}\left\{\frac{d}{dt}\mathbf{V_{Cqd}}\right\} \tag{3.28}$$

For simplicity, the transformed variables in frequency domain do not appear in the conventional form as $\mathbf{X(s)}$ and they are just simply expressed as $\mathbf{X}$.
All initial conditions are considered to be zero, simplifying and grouping like terms of (3.28):

$$\mathbf{i_{Cqd}} = \begin{bmatrix} Cs & \omega C \\ -\omega C & Cs \end{bmatrix} \mathbf{V_{Cqd}} \tag{3.29}$$

Now it can be defined the impedance of the current-voltage relationship for a capacitor in frequency-qd domain:

$$\mathbf{Z_C^{AM}} = \begin{bmatrix} Cs & \omega C \\ -\omega C & Cs \end{bmatrix}^{-1} \tag{3.30}$$

## 3.3 RL line model

The RL line model is comprised by a series resistor $R$ and an inductor $L$ connected between two buses $B_1$ and $B_2$.

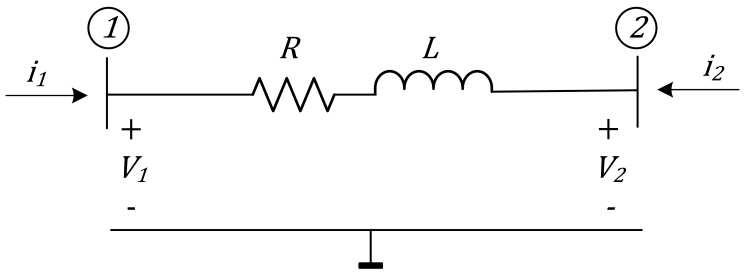


Figure 7: RL line

### 3.3.1 Admittance matrix model

The admittance matrix of the RL line is as follows:

$$\mathbf{Y_{RL}} = \begin{bmatrix} \mathbf{Y_L} & -\mathbf{Y_L} \\ -\mathbf{Y_L} & \mathbf{Y_L} \end{bmatrix}_{\mathbf{4x4}} \tag{3.31}$$

Where $Y_L$ is:

$$\mathbf{Y_L} = \begin{bmatrix} \frac{sL+R}{L^2s^2+L^2\omega^2+2\,LRs+R^2} & -\frac{L\omega}{L^2s^2+L^2\omega^2+2\,LRs+R^2} \\ \frac{L\omega}{L^2s^2+L^2\omega^2+2\,LRs+R^2} & \frac{sL+R}{L^2s^2+L^2\omega^2+2\,LRs+R^2} \end{bmatrix} \tag{3.32}$$

Relating the $Y_{RL}$ with node voltages $V$ and currents $I$:

$$\mathbf{Y_{RL}V} = \mathbf{I} \tag{3.33}$$

Where $V$ and $I$ are :

$$\mathbf{V} = \begin{bmatrix} \mathbf{V_{1qd}} \\ \mathbf{V_{2qd}} \end{bmatrix} \quad \mathbf{I} = \begin{bmatrix} \mathbf{i_{1qd}} \\ \mathbf{i_{2qd}} \end{bmatrix} \tag{3.34}$$

Substituting (3.31) and (3.34) in (3.33):

$$\begin{bmatrix} \mathbf{Y_L} & -\mathbf{Y_L} \\ -\mathbf{Y_L} & \mathbf{Y_L} \end{bmatrix} \begin{bmatrix} \mathbf{V_{1qd}} \\ \mathbf{V_{2qd}} \end{bmatrix} = \begin{bmatrix} \mathbf{i_{1qd}} \\ \mathbf{i_{2qd}} \end{bmatrix} \tag{3.35}$$

Where $V_{1qd}$, $V_{2qd}$ and $i_{1qd}$, $i_{2qd}$ are:

$$\begin{aligned} \mathbf{V_{1qd}} &= \begin{bmatrix} V_{1q} & V_{1d} \end{bmatrix}^T \quad \mathbf{V_{2qd}} = \begin{bmatrix} V_{2q} & V_{2d} \end{bmatrix}^T \\ \mathbf{i_{1qd}} &= \begin{bmatrix} i_{1q} & V_{1d} \end{bmatrix}^T \quad \mathbf{i_{2qd}} = \begin{bmatrix} i_{2q} & i_{2d} \end{bmatrix}^T \end{aligned} \tag{3.36}$$

### 3.3.2 State-space model

Applying Kirchhoff's voltage law to the RL line:

$$\mathbf{V_{1qd}} = R\,\mathbf{i_{Lqd}} + \mathbf{Z_L^{SS}}\mathbf{I_L^{SS}} + \mathbf{V_{2qd}} \tag{3.37}$$

Where $V_{1qd}$ and $V_{2qd}$ are:

$$\mathbf{V_{1qd}} = \begin{bmatrix} V_{1q} & V_{1d} \end{bmatrix}^T \quad \mathbf{V_{2qd}} = \begin{bmatrix} V_{2q} & V_{2d} \end{bmatrix}^T \tag{3.38}$$

And $i_{Lqd}$ and $I_L^{SS}$ are :

$$\mathbf{i_{Lqd}} = \begin{bmatrix} i_{Lq} & i_{Ld} \end{bmatrix}^T \quad \mathbf{I_L^{SS}} = \begin{bmatrix} \frac{d}{dt} i_{Lq} & \frac{d}{dt} i_{Ld} & i_{Lq} & i_{Ld} \end{bmatrix}^T \tag{3.39}$$

Substituting (3.14), (3.38) and (3.39) in (3.37), then solving for the derivatives of the currents and arranging them in matrix form it is obtained:

$$\begin{gathered} \frac{d}{dt}\begin{bmatrix} i_{Lq} \\ i_{Ld} \end{bmatrix} = \begin{bmatrix} -R/L & -\omega \\ \omega & -R/L \end{bmatrix}\begin{bmatrix} i_{Lq} \\ i_{Ld} \end{bmatrix} + \\ \begin{bmatrix} 1/L & 0 & -1/L & 0 \\ 0 & 1/L & 0 & -1/L \end{bmatrix}\begin{bmatrix} V_{1q} - V_{2q} \\ V_{1d} - V_{2d} \end{bmatrix} \end{gathered} \tag{3.40}$$

A state-space representation is described by the following set of equations:

$$\dot{x}(t) = \mathbf{A}x(t) + \mathbf{B}u(t) \quad y(t) = \mathbf{C}x(t) + \mathbf{D}u(t) \tag{3.41}$$

Based on (3.41), the coefficients of (3.40) are:

$$\begin{aligned} \mathbf{A} &= \begin{bmatrix} -R/L & -\omega \\ \omega & -R/L \end{bmatrix} & \mathbf{B} &= \begin{bmatrix} 1/L & 0 & -1/L & 0 \\ 0 & 1/L & 0 & -1/L \end{bmatrix} \\ \mathbf{C} &= [\mathbf{I_{2x2}}] & \mathbf{D} &= [\mathbf{0_{2x4}}] \end{aligned} \tag{3.42}$$

## 3.4 Pi line model

The AM and SS model of a distributed parameters Pi line in $qd0$-domain is described in this section. The pi line is connected between two buses $B_1$ and $B_2$.

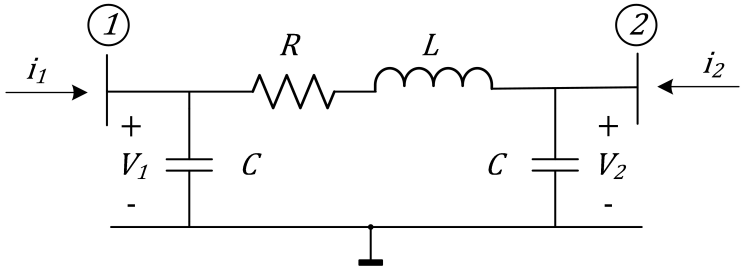


Figure 8: Pi line

### 3.4.1 Admittance matrix model

The admittance matrix for the Pi line model is as follows:

$$\mathbf{Y_{\Pi}} = \begin{bmatrix} \mathbf{Y_L} + \mathbf{Y_C} & -\mathbf{Y_L} \\ -\mathbf{Y_L} & \mathbf{Y_L} + \mathbf{Y_C} \end{bmatrix}_{\mathbf{4x4}} \tag{3.43}$$

Where $Y_C$ is:

$$\mathbf{Y_C} = \mathbf{Z_C^{AM}}^{-1} = \begin{bmatrix} Cs & \omega C \\ -\omega C & Cs \end{bmatrix} \tag{3.44}$$

Relating the $Y_{\Pi}$ with node voltages $V$ and currents $I$:

$$\mathbf{Y_{\Pi}V} = \mathbf{I} \tag{3.45}$$

Substituting (3.34) and (3.43) in (3.46):

$$\begin{bmatrix} \mathbf{Y_L} + \mathbf{Y_C} & -\mathbf{Y_L} \\ -\mathbf{Y_L} & \mathbf{Y_L} + \mathbf{Y_C} \end{bmatrix} \begin{bmatrix} \mathbf{V_{1qd}} \\ \mathbf{V_{2qd}} \end{bmatrix} = \begin{bmatrix} \mathbf{i_{1qd}} \\ \mathbf{i_{2qd}} \end{bmatrix} \tag{3.46}$$

### 3.4.2 State-space model

Applying Kirchhoff's voltage and current law to the pi line:

$$\begin{aligned} \mathbf{V_{1qd}} &= R\,\mathbf{i_{Lqd}} + \mathbf{Z_L^{SS}}\mathbf{I_L^{SS}} + \mathbf{V_{2qd}} \\ \mathbf{i_{1qd}} &= \mathbf{Z_C^{SS}}^{-1}\mathbf{V_{C1}^{SS}} + \mathbf{i_{Lqd}} \\ \mathbf{i_{2qd}} &= \mathbf{Z_C^{SS}}^{-1}\mathbf{V_{C2}^{SS}} - \mathbf{i_{Lqd}} \end{aligned} \tag{3.47}$$

The inputs of the system are $i_{1qd}$ and $i_{2qd}$. It is assumed that the current $i_{qd}$ flows from $V_{1qd}$ to $V_{2qd}$. Where $V_{C1}^{SS}$ and $V_{C2}^{SS}$ are :

$$\begin{aligned} \mathbf{V_{C1}^{SS}} &= \begin{bmatrix} \frac{d}{dt}V_{C1q} & \frac{d}{dt}V_{C1d} & V_{C1q} & V_{C1d} \end{bmatrix}^T \\ \mathbf{V_{C2}^{SS}} &= \begin{bmatrix} \frac{d}{dt}V_{C2q} & \frac{d}{dt}V_{C2d} & V_{C2q} & V_{C2d} \end{bmatrix}^T \end{aligned} \tag{3.48}$$

Substituting (3.14), (3.25), (3.39) and (3.48) in (3.47), solving for the derivatives and arranging the equations in state-space representation:

$$\mathbf{A} = \begin{bmatrix} -R/L & -\omega & 1/L & 0 & -1/L & 0 \\ \omega & -R/L & 0 & 1/L & 0 & -1/L \\ -1/C & 0 & 0 & -\omega & 0 & 0 \\ 0 & -1/C & \omega & 0 & 0 & 0 \\ 1/C & 0 & 0 & 0 & 0 & -\omega \\ 0 & 1/C & 0 & 0 & \omega & 0 \end{bmatrix}$$

$$\mathbf{B} = \begin{bmatrix} 0 & 0 & 0 & 0 \\ 0 & 0 & 0 & 0 \\ 1/C & 0 & 0 & 0 \\ 0 & 1/C & 0 & 0 \\ 0 & 0 & 1/C & 0 \\ 0 & 0 & 0 & 1/C \end{bmatrix} \quad \mathbf{C} = [\mathbf{I_{6x6}}] \quad \mathbf{D} = [\mathbf{0_{6x4}}] \tag{3.49}$$

## 3.5 Parallel pi lines model

The AM and SS model for two parallel pi lines in $qd0$-domain is described in this section. The two pi lines are connected between two buses $B_1$ and $B_2$.The procedure here described is similar to the previous ones, although, the main difference are the entering currents at every node that splits. It is of high importance to determine properly these currents for an accurate model of the system.

Fig. 9 depicts the parallel pi lines.

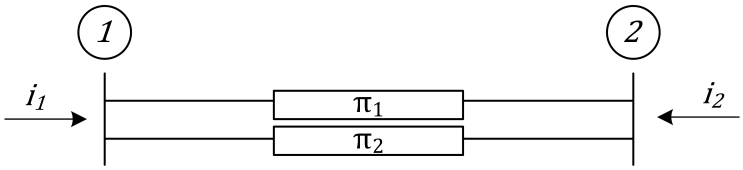


Figure 9: Parallel pi lines

### 3.5.1 Admittance matrix model

The admittance matrix for the two pi lines in parallel are as follow:

$$\mathbf{Y_{mat}} = \begin{bmatrix} \mathbf{Y_{L1}} + \mathbf{Y_{L2}} + \mathbf{Y_{C1}} + \mathbf{Y_{C2}} & -(\mathbf{Y_{L1}} + \mathbf{Y_{L2}}) \\ -(\mathbf{Y_{L1}} + \mathbf{Y_{L2}}) & \mathbf{Y_{L1}} + \mathbf{Y_{L2}} + \mathbf{Y_{C1}} + \mathbf{Y_{C2}} \end{bmatrix}_{\mathbf{4x4}} \tag{3.50}$$

Where $Y_{L1}$ and $Y_{L2}$ are the series inductor resistor admittances and $Y_{C1}$ and $Y_{C2}$ are the capacitor admittances of the lines. No further development of the equations is necessary because they have been developed on previous sections.

### 3.5.2 State-space model

Applying Kirchhoff's voltage law to the parallel pi lines:

$$\begin{aligned} \mathbf{V_{1qd}} &= R_1\, \mathbf{i_{L1qd}} + \mathbf{Z^{SS}_{L1} I^{SS}_{L1}} + \mathbf{V_{2qd}} \\ \mathbf{V_{1qd}} &= R_2\, \mathbf{i_{L2qd}} + \mathbf{Z^{SS}_{L2} I^{SS}_{L2}} + \mathbf{V_{2qd}} \end{aligned} \tag{3.51}$$

The currents $i_{1qd}$ and $i_{2qd}$ split when they enter the nodes at which the lines are connected. These split currents become unknowns to the system because there is not possible way to determine their values beforehand, therefore, a simplification is performed to disregard such split currents. The following procedure leaves a clearer evidence of the previously stated.

Considering that $i_{1qd}$ and $i_{2qd}$ are split in two different currents, then:

$$\mathbf{i_{1qd}} = \mathbf{i_{1x\_qd}} + \mathbf{i_{1y\_qd}} \quad \mathbf{i_{2qd}} = \mathbf{i_{2x\_qd}} + \mathbf{i_{2y\_qd}} \tag{3.52}$$

As it can be seen in Fig. (11) below the pi line 1 has been split by half to understand better the current flow, particularly, the current flowing through the inductor. As it is known, current

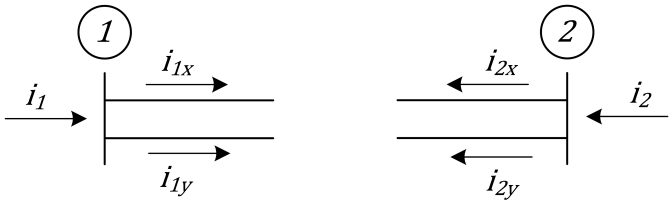


Figure 10: Split currents

flows from the higher to the lower potential, therefore, $i_{L1}$ enters the node of the second half and leaves the node of the first half of the pi line 1. This reasoning is applied for the more complex networks developed in this thesis.

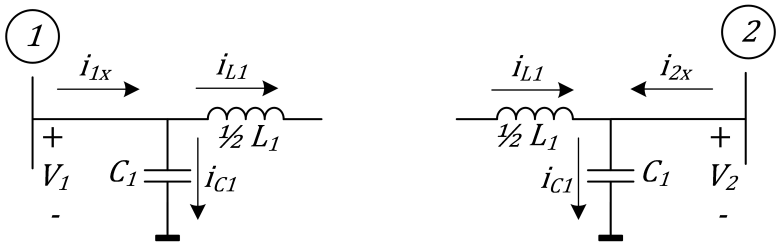


Figure 11: Node currents

Applying Kirchhoff's current law at every node, the following equations are obtained:

$$\begin{aligned}
\mathbf{i_{1x_qd}} &= \mathbf{Z_{C1}^{SS}}^{-1}\mathbf{V_{C1}^{SS}} + \mathbf{i_{L1qd}} \\
\mathbf{i_{2x_qd}} &= \mathbf{Z_{C1}^{SS}}^{-1}\mathbf{V_{C2}^{SS}} - \mathbf{i_{L1qd}} \\
\mathbf{i_{1y_qd}} &= \mathbf{Z_{C2}^{SS}}^{-1}\mathbf{V_{C1}^{SS}} + \mathbf{i_{L2qd}} \\
\mathbf{i_{2y_qd}} &= \mathbf{Z_{C2}^{SS}}^{-1}\mathbf{V_{C2}^{SS}} - \mathbf{i_{L2qd}}
\end{aligned} \tag{3.53}$$

Substituting (3.53) in (3.52) and arranging the equations:

$$\begin{aligned}
\mathbf{i_{1qd}} &= \left(\mathbf{Z_{C1}^{SS}}^{-1} + \mathbf{Z_{C2}^{SS}}^{-1}\right)\mathbf{V_{C1}^{SS}} + \mathbf{i_{L1qd}} + \mathbf{i_{L2qd}} \\
\mathbf{i_{2qd}} &= \left(\mathbf{Z_{C1}^{SS}}^{-1} + \mathbf{Z_{C2}^{SS}}^{-1}\right)\mathbf{V_{C2}^{SS}} - \mathbf{i_{L1qd}} - \mathbf{i_{L2qd}}
\end{aligned} \tag{3.54}$$

Once that the $I_{nx}$ and $I_{ny}$ terms are substituted, it can be seen that the Kirchhoff´s current law for every node is given by the currents entering and leaving the node plus the sum of the impedances of the capacitors times the voltage of the respective node.
Where $V_{1qd}$ and $V_{2qd}$ are the node voltages, therefore :

$$\mathbf{V_{C1qd}} = \mathbf{V_{1qd}} \quad \mathbf{V_{C2qd}} = \mathbf{V_{2qd}} \tag{3.55}$$

The state-space representation in matrix form is not depicted, because it has been developed on previous sections. Therefore, it is only expressed through equations.

This section of parallel pi lines develops the method utilized for the determination of the current flows in SS modeling when lines are connected in parallel or at least one end of many lines are connected to the same node. Consider that these procedures are no required for the AM modeling, clearly this an advantage of the AM modeling over the SS modeling. In fact, the AM modeling it is a fast and well known procedure for obtaining the admittance of any network.

Finally, networks with more complex topologies are modeled in the following sections, the procedures here developed hold for those topologies too. Moreover,the topology complexity it is increased gradually to fully understand the modelling technique.

## 3.6 Three bus network

A three bus network model is developed in $qd0$-domain. The network is comprised by three pi power lines, every power line connects two buses and every line shares two buses with the other line, creating a triangular shape. It is a small system that shows the modelling procedures that are going to be applied for the next networks.

Fig. 13 depicts the three bus network.

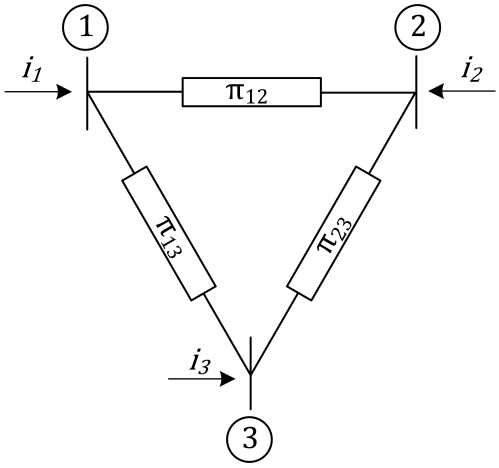


Figure 12: Three bus network

### 3.6.1 Admittance matrix model

Obtaining the admittance matrix $Y_{3B}$:

$$\mathbf{Y_{3B}} = \begin{bmatrix} \mathbf{Y_{11}} & -Y_{L12} & -Y_{L13} \\ -Y_{L12} & \mathbf{Y_{22}} & -Y_{L23} \\ -Y_{L13} & -Y_{L23} & \mathbf{Y_{33}} \end{bmatrix}_{\mathbf{6x6}} \tag{3.56}$$

Where $Y_{11}$, $Y_{22}$ and $Y_{33}$ are:

$$\begin{aligned}\mathbf{Y_{11}} &= Y_{L12} + Y_{L13} + Y_{C12} + Y_{C13}\\ \mathbf{Y_{22}} &= Y_{L12} + Y_{L23} + Y_{C12} + Y_{C23}\\ \mathbf{Y_{33}} &= Y_{L13} + Y_{L23} + Y_{C13} + Y_{C23}\end{aligned} \tag{3.57}$$

Arranging (3.56) in the current-voltage relationship form:

$$[\mathbf{Y_{3B}}] \begin{bmatrix} \mathbf{V_{1qd}} \\ \mathbf{V_{2qd}} \\ \mathbf{V_{3qd}} \end{bmatrix} = \begin{bmatrix} \mathbf{i_{1qd}} \\ \mathbf{i_{2qd}} \\ \mathbf{i_{3qd}} \end{bmatrix} \tag{3.58}$$

### 3.6.2 State-space model

Applying Kirchhoff's voltage law:

$$\begin{aligned}\mathbf{V_{1qd}} &= R_{12}\,\mathbf{i_{L12qd}} + \mathbf{Z^{SS}_{L12}}\mathbf{I^{SS}_{L12}} + \mathbf{V_{2qd}}\\ \mathbf{V_{1qd}} &= R_{13}\,\mathbf{i_{L13qd}} + \mathbf{Z^{SS}_{L13}}\mathbf{I^{SS}_{L13}} + \mathbf{V_{3qd}}\\ \mathbf{V_{2qd}} &= R_{23}\,\mathbf{i_{L23qd}} + \mathbf{Z^{SS}_{L23}}\mathbf{I^{SS}_{L23}} + \mathbf{V_{3qd}}\end{aligned} \tag{3.59}$$

Applying Kirchhoff's current law:

$$\begin{aligned}\mathbf{i_{1qd}} &= \mathbf{i_{L12qd}} + \mathbf{i_{L13qd}} + \left(\mathbf{Z^{SS}_{C12}}^{-1} + \mathbf{Z^{SS}_{C13}}^{-1}\right)\mathbf{V^{SS}_{C1}}\\ \mathbf{i_{2qd}} &= -\mathbf{i_{L12qd}} + \mathbf{i_{L23qd}} + \left(\mathbf{Z^{SS}_{C12}}^{-1} + \mathbf{Z^{SS}_{C23}}^{-1}\right)\mathbf{V^{SS}_{C2}}\\ \mathbf{i_{3qd}} &= -\mathbf{i_{L13qd}} - \mathbf{i_{L23qd}} + \left(\mathbf{Z^{SS}_{C13}}^{-1} + \mathbf{Z^{SS}_{C23}}^{-1}\right)\mathbf{V^{SS}_{C3}}\end{aligned} \tag{3.60}$$

An arbitrary path must be chosen in order to obtain the proper current flow in the network for the SS model. It is assumed that the current flow path follows the following scheme based on the voltage level at the buses, where $V_{B1} > V_{B2} > V_{B3}$. Therefore, the chosen current flow $i_{flow}$ goes from the first bus $B_1$, passes by the second bus $B_2$ and it ends at the third bus $B_3$, in numerical order. Also, the current flow goes from the first bus $B_1$ to the third bus $B_3$ directly. This is obvious because the current $i_1$ when it enters at the bus $B_1$ splits in two. Fig. (13) depicts this arbitrary current flow path.

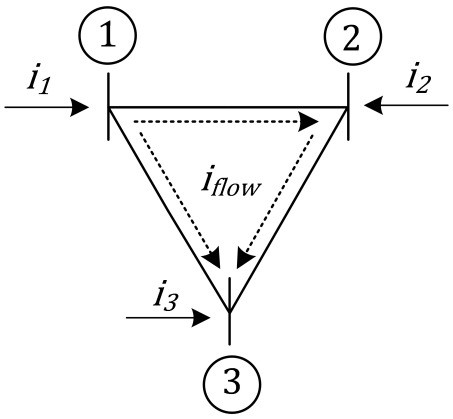


Figure 13: Current flow path for the three bus network

It is worth mentioning that the chosen path can be easily inferred from (3.59), although, it is important to leave proof of the proposed methodology.

Additionally, the current flow procedure described is easy to demonstrate applying the Kirchhoff's current law. By definition: it states that the algebraic sum of currents entering a node (or a closed boundary) is zero [19]. Mathematically, KCL implies that

$$\sum_{n=1}^{N} i_n = 0$$

where $N$ is the number of branches connected to the node and $i_n$ is the $n$th current entering (or leaving) the node.

Considering that the sum of the three currents that enter into the network must be zero and (3.60) is considered. Which is formed by a set of three equations and are summed up without taken into account the currents flowing through the capacitors. The following result is obtained:

$$\mathbf{i_{1qd}} + \mathbf{i_{2qd}} + \mathbf{i_{3qd}} = \mathbf{i_{L12qd}} + \mathbf{i_{L13qd}} - \mathbf{i_{L12qd}} + \mathbf{i_{L23qd}} - \mathbf{i_{L13qd}} - \mathbf{i_{L23qd}}$$
$$\mathbf{i_{1qd}} + \mathbf{i_{2qd}} + \mathbf{i_{3qd}} = 0$$

As it can be seen from the equations above, every term on the right side of the first equation cancels out and the sum of the currents is zero. This is enough proof that the procedure here discussed is correct and complies with KCL. For clarification, the currents flowing through the capacitors are not considered because they go to ground and do not affect the current flow into the network.

## 3.7 Four bus network

A four bus network model is developed in $qd0$-domain. The network is comprised by five pi power lines, every power line connects two buses and every line shares two buses. Fig. 14 depicts the four bus network.

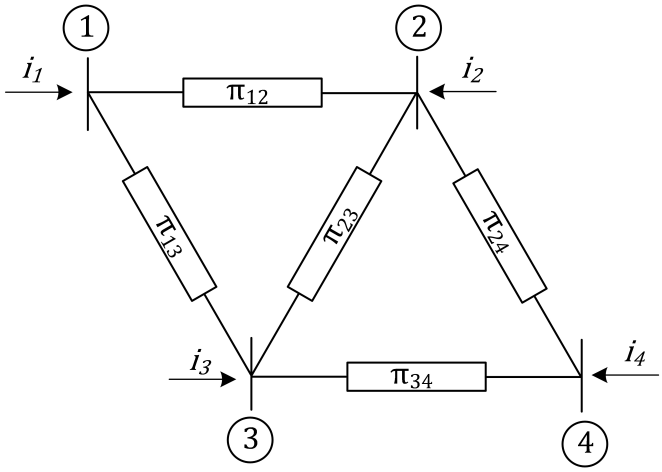


Figure 14: Four bus network

### 3.7.1 Admittance matrix model

Obtaining the admittance matrix $Y_{4B}$:

$$\mathbf{Y_{4B}} = \begin{bmatrix} \mathbf{Y_{11}} & -Y_{L12} & -Y_{L13} & [0_{2\times2}] \\ -Y_{L12} & \mathbf{Y_{22}} & -Y_{L23} & -Y_{L24} \\ -Y_{L13} & -Y_{L23} & \mathbf{Y_{33}} & -Y_{L34} \\ [0_{2\times2}] & -Y_{L24} & -Y_{L34} & \mathbf{Y_{44}} \end{bmatrix}_{\mathbf{8\times8}} \tag{3.61}$$

Where $Y_{11}$, $Y_{22}$, $Y_{33}$ and $Y_{44}$ are:

$$\begin{aligned} \mathbf{Y_{11}} &= Y_{L12} + Y_{L13} + Y_{C12} + Y_{C13} \\ \mathbf{Y_{22}} &= Y_{L12} + Y_{L23} + Y_{L24} + Y_{C12} + Y_{C23} + Y_{C24} \\ \mathbf{Y_{33}} &= Y_{L13} + Y_{L23} + Y_{L34} + Y_{C13} + Y_{C23} + Y_{C34} \\ \mathbf{Y_{44}} &= Y_{L24} + Y_{L34} + Y_{C24} + Y_{C34} \end{aligned} \tag{3.62}$$

Arranging (3.61) in the current-voltage relationship form:

$$[\mathbf{Y_{4B}}] \begin{bmatrix} \mathbf{V_{1qd}} \\ \mathbf{V_{2qd}} \\ \mathbf{V_{3qd}} \\ \mathbf{V_{4qd}} \end{bmatrix} = \begin{bmatrix} \mathbf{i_{1qd}} \\ \mathbf{i_{2qd}} \\ \mathbf{i_{3qd}} \\ \mathbf{i_{4qd}} \end{bmatrix} \tag{3.63}$$

### 3.7.2 State-space model

Applying Kirchhoff's voltage law:

$$\begin{aligned}
\mathbf{V_{1qd}} &= R_{12}\,\mathbf{i_{L12qd}} + \mathbf{Z^{SS}_{L12}}\mathbf{I^{SS}_{L12}} + \mathbf{V_{2qd}} \\
\mathbf{V_{1qd}} &= R_{13}\,\mathbf{i_{L13qd}} + \mathbf{Z^{SS}_{L13}}\mathbf{I^{SS}_{L13}} + \mathbf{V_{3qd}} \\
\mathbf{V_{2qd}} &= R_{23}\,\mathbf{i_{L23qd}} + \mathbf{Z^{SS}_{L23}}\mathbf{I^{SS}_{L23}} + \mathbf{V_{3qd}} \\
\mathbf{V_{2qd}} &= R_{24}\,\mathbf{i_{L24qd}} + \mathbf{Z^{SS}_{L24}}\mathbf{I^{SS}_{L24}} + \mathbf{V_{4qd}} \\
\mathbf{V_{3qd}} &= R_{34}\,\mathbf{i_{L34qd}} + \mathbf{Z^{SS}_{L34}}\mathbf{I^{SS}_{L34}} + \mathbf{V_{4qd}}
\end{aligned} \tag{3.64}$$

Applying Kirchhoff's current law:

$$\begin{aligned}
\mathbf{i_{1qd}} &= \mathbf{i_{L12qd}} + \mathbf{i_{L13qd}}\,(\mathbf{t}) + \left(\mathbf{Z^{SS}_{C12}}^{-1} + \mathbf{Z^{SS}_{C13}}^{-1}\right)\mathbf{V^{SS}_{C1}} \\
\mathbf{i_{2qd}} &= -\mathbf{i_{L12qd}} + \mathbf{i_{L23qd}} + \mathbf{i_{L24qd}} \\
&\quad + \left(\mathbf{Z^{SS}_{C12}}^{-1} + \mathbf{Z^{SS}_{C23}}^{-1} + \mathbf{Z^{SS}_{C24}}^{-1}\right)\mathbf{V^{SS}_{C2}} \\
\mathbf{i_{3qd}} &= -\mathbf{i_{L13qd}} - \mathbf{i_{L23qd}} + \mathbf{i_{L34qd}} \\
&\quad + \left(\mathbf{Z^{SS}_{C13}}^{-1} + \mathbf{Z^{SS}_{C23}}^{-1} + \mathbf{Z^{SS}_{C34}}^{-1}\right)\mathbf{V^{SS}_{C3}} \\
\mathbf{i_{4qd}} &= -\mathbf{i_{L24qd}} - \mathbf{i_{L34qd}} + \left(\mathbf{Z^{SS}_{C24}}^{-1} + \mathbf{Z^{SS}_{C34}}^{-1}\right)\mathbf{V^{SS}_{C4}}
\end{aligned} \tag{3.65}$$

The procedure of the SS modeling for the four bus network is similar to the one used in the three bus network. The complexity of the network increases a few by adding two more lines and one extra bus. Special care needs to be put on the chosen current flow path because if it is done incorrectly, it would provide a bad model of the system.

Again, it is assumed that the current flow path follows the following scheme based on the voltage level at the buses, where $V_{B1} > V_{B2} > V_{B3} > V_{B4}$. Fig. 15 clarifies better the chosen current flow path $i_{flow\_1}$ and $i_{flow\_2}$ for the network.

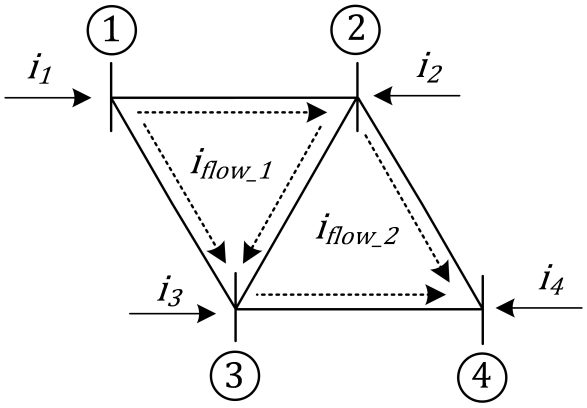


Figure 15: Current flow path for the four bus network

## 3.8 Five bus network

Previously it was described the methodology used to model power networks in $qd0$-domain. The network of interest for this thesis is a five bus network comprised by seven pi power lines of different lengths. The proposed network in this thesis is taken from the Cigre 14-bus model benchmark [1]. The 14-bus network is comprised by two networks operating at different voltage levels. For the sake of simplicity, the network has been reduced and only the topology of the 220 kV network is considered in this thesis. The 110 kV network is represented by means of a Thevenin equivalent connected to the bus number 4 of the 220 kV network. Fig. 16 shows the 220 kV five bus network without the Thevenin equivalent, this will be added later.

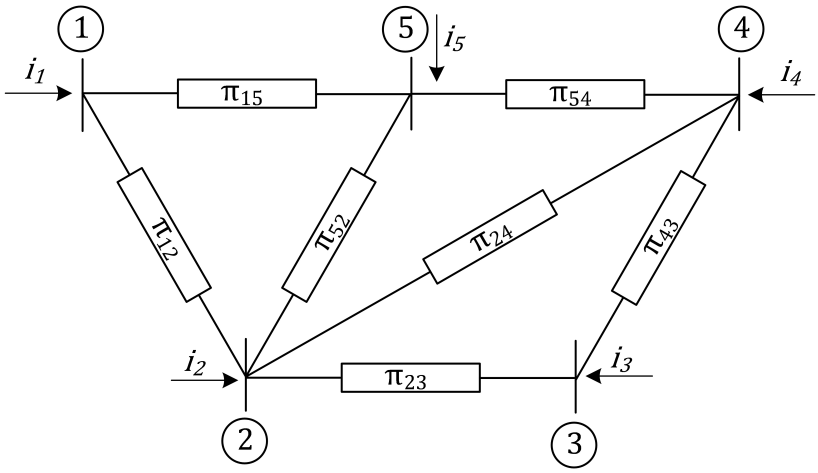


Figure 16: Five bus network

### 3.8.1 Admittance matrix model

Obtaining the admittance matrix $Y_{5B}$ of the network:

$$\mathbf{Y_{5B}} = \begin{bmatrix} \mathbf{Y_{11}} & -Y_{L12} & [0_{2\times2}] & [0_{2\times2}] & -Y_{L15} \\ -Y_{L12} & \mathbf{Y_{22}} & -Y_{L23} & -Y_{L24} & -Y_{L52} \\ [0_{2\times2}] & -Y_{L23} & \mathbf{Y_{33}} & -Y_{L43} & [0_{2\times2}] \\ [0_{2\times2}] & -Y_{L24} & -Y_{L43} & \mathbf{Y_{44}} & -Y_{L54} \\ -Y_{L15} & -Y_{L52} & [0_{2\times2}] & -Y_{L54} & \mathbf{Y_{55}} \end{bmatrix}_{\mathbf{10\times10}} \tag{3.66}$$

Where $Y_{11}$, $Y_{22}$, $Y_{33}$, $Y_{44}$ and $Y_{55}$ are:

$$\begin{aligned} \mathbf{Y_{11}} &= Y_{L12} + Y_{L15} + Y_{C12} + Y_{C15} \\ \mathbf{Y_{22}} &= Y_{L12} + Y_{L23} + Y_{L24} + Y_{L52} + Y_{C12} + Y_{C23} + Y_{C24} + Y_{C52} \\ \mathbf{Y_{33}} &= Y_{L23} + Y_{L43} + Y_{C23} + Y_{C43} \\ \mathbf{Y_{44}} &= Y_{L24} + Y_{L43} + Y_{L54} + Y_{C24} + Y_{C43} + Y_{C54} \\ \mathbf{Y_{55}} &= Y_{L15} + Y_{L52} + Y_{L54} + Y_{C15} + Y_{C52} + Y_{C54} \end{aligned} \tag{3.67}$$

Arranging (3.66) in the current-voltage relationship form:

$$[\mathbf{Y_{5B}}]\begin{bmatrix}\mathbf{V_{1qd}}\\ \mathbf{V_{2qd}}\\ \mathbf{V_{3qd}}\\ \mathbf{V_{4qd}}\\ \mathbf{V_{5qd}}\end{bmatrix}=\begin{bmatrix}\mathbf{i_{1qd}}\\ \mathbf{i_{2qd}}\\ \mathbf{i_{3qd}}\\ \mathbf{i_{4qd}}\\ \mathbf{i_{5qd}}\end{bmatrix} \tag{3.68}$$

### 3.8.2 State-space model

Applying Kirchhoff's voltage law:

$$\begin{aligned}
\mathbf{V_{1qd}} &= R_{12}\,\mathbf{i_{L12qd}} + \mathbf{Z^{SS}_{L12}}\mathbf{I^{SS}_{L12}} + \mathbf{V_{2qd}}\\
\mathbf{V_{1qd}} &= R_{15}\,\mathbf{i_{L15qd}} + \mathbf{Z^{SS}_{L15}}\mathbf{I^{SS}_{L15}} + \mathbf{V_{5qd}}\\
\mathbf{V_{5qd}} &= R_{52}\,\mathbf{i_{L52qd}} + \mathbf{Z^{SS}_{L52}}\mathbf{I^{SS}_{L52}} + \mathbf{V_{2qd}}\\
\mathbf{V_{2qd}} &= R_{24}\,\mathbf{i_{L24qd}} + \mathbf{Z^{SS}_{L24}}\mathbf{I^{SS}_{L24}} + \mathbf{V_{4qd}}\\
\mathbf{V_{2qd}} &= R_{23}\,\mathbf{i_{L23qd}} + \mathbf{Z^{SS}_{L23}}\mathbf{I^{SS}_{L23}} + \mathbf{V_{3qd}}\\
\mathbf{V_{5qd}} &= R_{54}\,\mathbf{i_{L54qd}} + \mathbf{Z^{SS}_{L54}}\mathbf{I^{SS}_{L54}} + \mathbf{V_{4qd}}\\
\mathbf{V_{4qd}} &= R_{43}\,\mathbf{i_{L43qd}} + \mathbf{Z^{SS}_{L43}}\mathbf{I^{SS}_{L43}} + \mathbf{V_{3qd}}
\end{aligned} \tag{3.69}$$

Applying Kirchhoff's current law:

$$\begin{aligned}
\mathbf{i_{1qd}} &= \mathbf{i_{L12qd}} + \mathbf{i_{L15qd}} + \left(\mathbf{Z^{SS}_{C12}}^{-1} + \mathbf{Z^{SS}_{C15}}^{-1}\right)\mathbf{V^{SS}_{C1}}\\
\mathbf{i_{2qd}} &= -\mathbf{i_{L12qd}} - \mathbf{i_{L52qd}} + \mathbf{i_{L23qd}} + \mathbf{i_{L24qd}}\\
&\quad + \left(\mathbf{Z^{SS}_{C12}}^{-1} + \mathbf{Z^{SS}_{C23}}^{-1} + \mathbf{Z^{SS}_{C24}}^{-1} + \mathbf{Z^{SS}_{C52}}^{-1}\right)\mathbf{V^{SS}_{C2}}\\
\mathbf{i_{3qd}} &= -\mathbf{i_{L23qd}} - \mathbf{i_{L43qd}} + \left(\mathbf{Z^{SS}_{C23}}^{-1} + \mathbf{Z^{SS}_{C43}}^{-1}\right)\mathbf{V^{SS}_{C3}}\\
\mathbf{i_{4qd}} &= -\mathbf{i_{L54qd}} - \mathbf{i_{L24qd}} + \mathbf{i_{L43qd}}\\
&\quad + \left(\mathbf{Z^{SS}_{C54}}^{-1} + \mathbf{Z^{SS}_{C24}}^{-1} + \mathbf{Z^{SS}_{C43}}^{-1}\right)\mathbf{V^{SS}_{C4}}\\
\mathbf{i_{5qd}} &= -\mathbf{i_{L15qd}} + \mathbf{i_{L52qd}} + \mathbf{i_{L54qd}}\\
&\quad + \left(\mathbf{Z^{SS}_{C15}}^{-1} + \mathbf{Z^{SS}_{C52}}^{-1} + \mathbf{Z^{SS}_{C54}}^{-1}\right)\mathbf{V^{SS}_{C5}}
\end{aligned} \tag{3.70}$$

The procedure for obtaining both models is equal to the ones already discussed. Although, there is a slight change in the selection of the current flow, it is important to remind that this is an arbitrary selection. For this network the chosen path of the current flow differs from what has been chosen previously. Given that in the three and four bus networks the highest voltage level corresponded to the first bus and the lowest voltage level corresponded to the last bus. Due to this reason, the current flow followed a numerical order.

In this case, it is assumed that the current flow path follows the following scheme based on the voltage level at the buses, where $V_{B1} > V_{B5} > V_{B2} > V_{B4} > V_{B3}$. As a reminder, the current flow path can also be inferred from (3.69).

## 3.9 Equivalent network

The model of the AM and SS representation of the equivalent network is developed in this section. The equivalent network is depicted in Fig. 17 by a voltage source in series with a series resistor inductor.

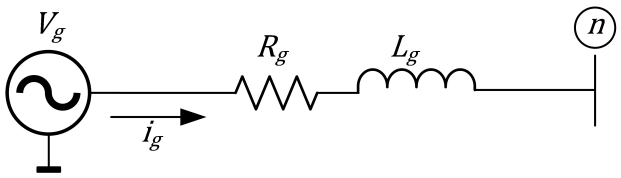


Figure 17: Equivalent network

### 3.9.1 Admittance matrix model

The AM model for the equivalent network is easy and simple to model, it is given by the current-voltage relationship.

$$\left[\mathbf{Y_g}\right]\left[\mathbf{V_{g\_qd}}\right] = \left[\mathbf{i_{g\_qd}}\right] \tag{3.71}$$

Where $Y_g$ is:

$$\mathbf{Y_g} = \mathbf{Z_g^{AM^{-1}}} = \begin{bmatrix} L_g s & \omega L_g \\ -\omega L_g & L_g s \end{bmatrix}^{-1} \tag{3.72}$$

### 3.9.2 State-space model

The SS model of the equivalent network is similar to the SS model of the RL line.

$$\mathbf{V_{g\_qd}} = R_g\, \mathbf{i_{Lg\_qd}} + \mathbf{Z_{Lg}^{SS}} \mathbf{I_{Lg}^{SS}} + \mathbf{V_{n\_qd}} \tag{3.73}$$

The modelling description finishes with the model of the equivalent network. As can be seen from what has been developed through all this section, the modelling procedures require the utilization of some mathematical tools. It is important to realize that these procedures are normally performed by means of software programs which simplify all the calculation times and difficulties.

For example, the algorithm for the calculation of the admittance matrix it is well known and it is easily programmable. Whereas, the state-space representation takes more time if it is hand calculated and requires more complex algorithms if it is calculated by means of software programs. Of course, both methods are equivalent.

# 4 Comparison of the state-space and the admittance matrix

The comparison of the modelling techniques detailed in the previous section is highly important, because it demonstrates that both approaches are equivalent. The mathematical tools utilized to compare the models are the eigenvalues and singular values.

## 4.1 Eigenvalues

The eigenvalues give important information of the characteristic response of a system in time. Moreover, it allows to determine the stability of the system itself. For power network applications, the eigenvalues are obtained from the $Y_{mat}$ and from the $\mathbf{A}$ coefficient matrix of the state-space model.
In section 2.3 was introduced the term transfer function, which is a rational function in the complex frequency $s$. A transfer function $H(s)$ is given by the following expression [2]:

$$H(s) = \frac{N(s)}{D(s)} = \frac{b_m s^m + b_{m-1}s^{m-1} + \ldots + b_1 s + b_0}{a_n s^n + a_{n-1}s^{n-1} + \ldots + a_1 s + a_0} \tag{4.1}$$

where $N(s)$ and $D(s)$ are polynomials with real coefficients. If such polynomials are factorized, then:

$$H(s) = \frac{N(s)}{D(s)} = K\frac{(s-z_1)(s-z_2)\ldots(s-z_{m-1})(s-z_m)}{(s-p_1)(s-p_2)\ldots(s-p_{m-1})(s-p_m)} \tag{4.2}$$

where $K = b_m/a_n$ [2], the $z_i$ terms are called zeros and are the roots of the polynomial $N(s)$, when $N(s) = 0$. The $p_i$ terms are called *poles* and are the roots of the polynomial $D(s)$, when $D(s) = 0$. The poles and zeros must be either purely real, or appear in complex conjugate pairs.

To obtain the eigenvalues of the state-space model two expressions can be used, but, both are equivalent. The first expression is described by the equation (2.20), where the eigenvalues are found in the poles of the denominator of the transfer function $H^{SS}(s)$ of the state-space model.

$$\mathbf{H^{SS}}(s) = \mathbf{C}(s\mathbf{I} - \mathbf{A})^{-1}\mathbf{B}$$

And the second one, it is to obtain the characteristic polynomial $P_A(\lambda)$ of the $\mathbf{A}$ coefficient matrix of the state-space system, which roots are the eigenvalues $\lambda$ of the system. The characteristic polynomial is found in the determinant of the $\mathbf{A}$ coefficient matrix and it is given by the following expression [23]:

$$P_A(\lambda) = det\,[\lambda\mathbf{I} - \mathbf{A}] = 0 \tag{4.3}$$

Finally, it is important to remember that in order to compare both systems, it is not the admittance matrix $Y_{mat}$ but the impedance matrix $Z_{mat}$ the one to be used. Therefore, the zeros instead of the poles are the ones to be considered.

## 4.2 Singular values

The singular values are obtained from the singular value decomposition (SVD), which is a special factorization for a $m \times n$ matrix **A**. This algorithm allows to factorize non-square matrices. However, the main goal is not to obtain the decomposition but the singular values.

Consider the $n \times n$ matrix $A^T A$, which is symmetric, therefore, its eigenvalues are real.

**Lemma.** If $\lambda$ is an eigenvalue of $A^T A$, then $\lambda \geq 0$ [20].

Let $\lambda_1, \ldots, \lambda_n$ denote the eigenvalues of $A^T A$, with repetitions. Order these so that $\lambda_1 \geq \lambda_2 \geq \cdots \geq \lambda_n \geq 0$. Let $\sigma_i = \sqrt{\lambda_i}$, so that $\sigma_1 \geq \sigma_2 \geq \cdots \geq \sigma_n \geq 0$. The numbers $\sigma_1 \geq \sigma_2 \geq \cdots \geq \sigma_n$ defined above are called the singular values of A.

The main reason to obtain the singular values, it is because reduces and simplifies the data provided. For the thesis purposes, it is important to notice that the singular values $\sigma_i$ are function of the complex frequency $s$, where $s = j\omega$. This allows to make a frequency sweep of the singular values to spot possible peaks of resonance along a given frequency range. In some manner, this methodology to identify peaks of resonance resembles that of a bode plot. Although, singular values provides a better data management.

The comparisons are performed by means of MATLAB R2019a. The MATLAB functions utilized for obtaining the plots for the eigenvalues and singular values are the following:

- The **eig(A)** function, which returns a column vector containing the eigenvalues of square matrix A [24].
- The **sigma(SYS,{WMIN,WMAX})**, which produces a singular value plot of the frequency response of the dynamic system SYS, for the range of specified frequencies [25].

It is important to note that a matrix is a change in magnitude and direction of the input vector. Both the eigenvalues and singular values show the change in magnitude, which allows to identified the resonances of a linear system [26].

## 4.3 Graphic comparison of the state-space and admittance matrix models

To apply and demonstrate graphically that both models are equivalent, two figures are shown. Fig. 18 shows the singular values of both models for the five bus network and Fig. 19 shows the eigenvalues of both models for the five bus network. As it can be seen, both models match each other demonstrating graphically their equivalence and it can be expected the same dynamic response in time.

Consider that the $Z_{mat} = 1/Y_{mat}$ of the five bus network derived by means of the admittance matrix is being compared with the **A** matrix of the state-space model of the five bus network.

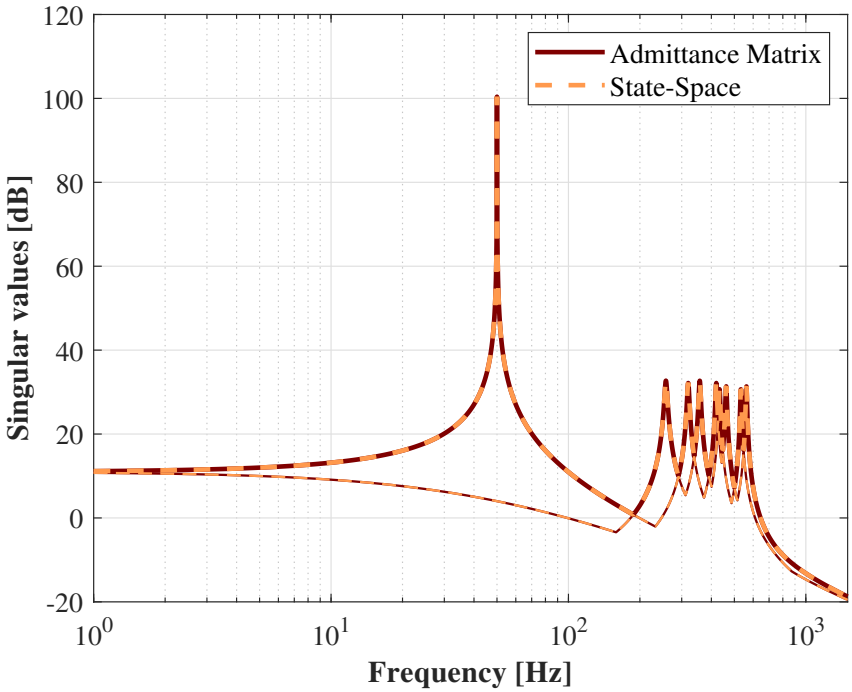


Figure 18: Singular values of the five bus network

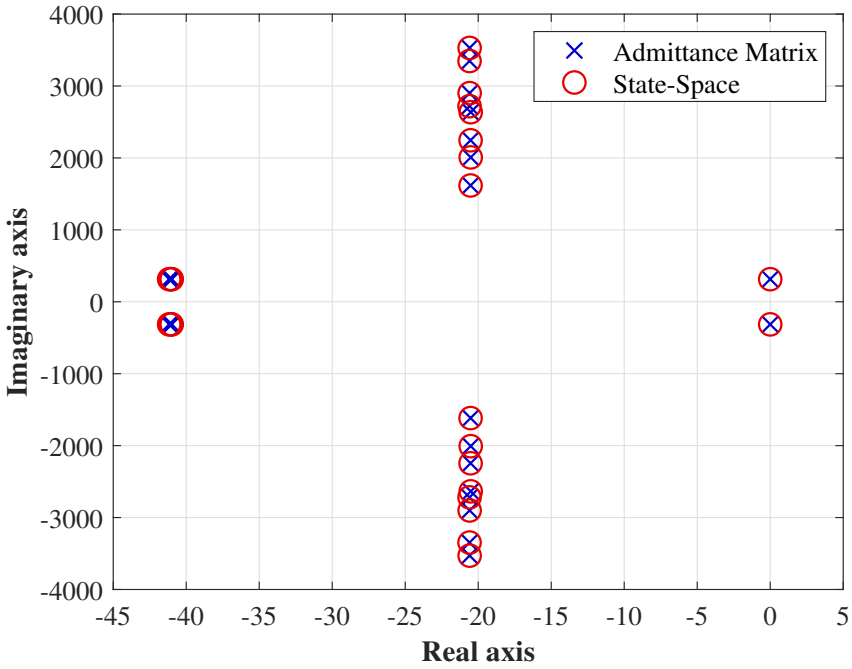


Figure 19: Eigenvalues of the five bus network

# 5 Power system parameters

In section 3 was introduced and developed the modelling techniques for obtaining the model of a power network in $qd0$-domain using the State-space representation and the admittance matrix. In Section 3.8 was introduced the five bus network topology, which is the one that comprises the power system of interest in this thesis.

In this section it is described completely the technical characteristics of the power system to be studied, which is comprised by the overhead lines (OHL) of the five bus network, the grid-connected voltage source converter and the Thevenin equivalent of the network. No load is considered, because the main objective is to study the interactions of the power network with the VSC converter.

Future simulations are performed using the parameters here detailed. Fig. 20 depicts the complete power system.

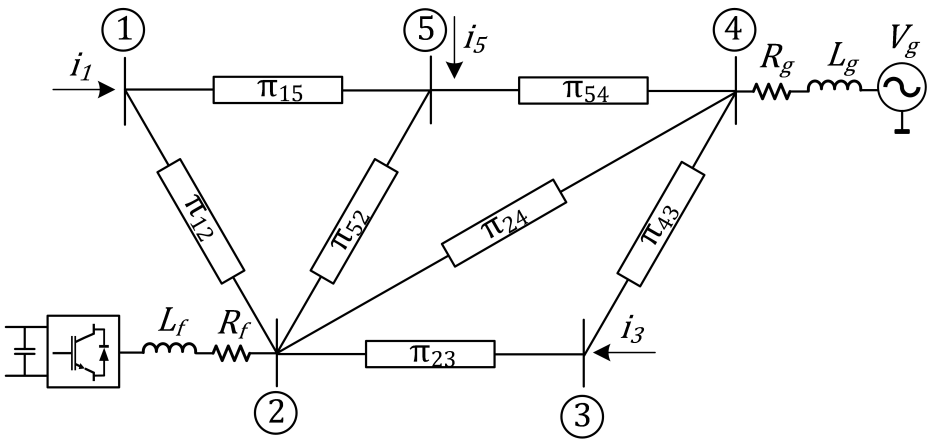


Figure 20: Five bus network with VSC converter and Thevenin equivalent

Although it is not depicted in Fig. 20, there is a power transformer between the grid and the VSC converter. The values for the converter filter resistance $R_f$ and converter filter inductance $L_f$ already include the corresponding impedance of the power transformer.

The procedures and equations applied for calculating the parameters in Tables 2, 3 and 4 can be found in the Appendices 7.5, 7.6 and 7.7, respectively. Parameters of Table 1 and the DC resistance, GMR and outer radius of Table 2 were taken from [1].

The OHL parameters are given in Table 1. Due to the length of the OHL, distributed parameters are considered for the power lines. In Table 2, it can be found the general OHL distributed parameters.

Table 1: 220 kV OHL parameters [1]

| Parameter | Data |
|---|---|
| Conductors per phase | 1 |
| Shield Wires | No |
| Phase A coordinates (m) | (-8.05, 16.4) |
| Phase B coordinates (m) | (0, 16.4) |
| Phase C coordinates (m) | (8.05, 16.4) |
| Phase Transposition (m) | Yes (perfect symmetry) |
| Soil Resistivity (Ωm) | 400 |
| Conductor | 600 ACSR Curlew |

Table 2: General OHL distributed parameters

| Parameter | Symbol | Value | Units |
|---|---|---|---|
| DC resistance | $R$ | 0.05527 | $\Omega/\mathrm{km}$ |
| Geometric mean radius | $GMR$ | 12.75733 | mm |
| Outer radius | $r_{cond}$ | 15.8115 | mm |
| Geometric mean distance | $GMD$ | 10.1424 | m |
| Inductance | $L$ | 1.3357 | mH/km |
| Capacitance | $C$ | 8.5950 | nF/km |
| Inductive reactance | $X_L$ | 0.4196 | $\Omega/\mathrm{km}$ |
| Capacitive reactance | $X_C$ | $2.7002 \times 10^{-6}$ | S/km |
| Impedance | $Z$ | 0.0552+j0.4196 | $\Omega/\mathrm{km}$ |
| Admittance | $Y$ | j$2.7002 \times 10^{-6}$ | S/km |
| Propagation constant | $\gamma$ | 0.00007+j0.00107 | |

In Table 3, it can be found the distributed parameters for every OHL . Such parameters are in per unit (pu), the chosen bases for obtaining the pu values are $S_{base} = 100\,\mathrm{MVA}$ and $V_{base} = 220\,\mathrm{kV}$. Note that at the bottom of the table, $Z_{base}$ and $Y_{base}$ are given. Consider that in this thesis the units of many variables or physical quantities are expressed in per unit and the bases here defined applied for all of them, unless otherwise specified.

Table 3: OHL distributed parameters

| Lines | Length (km) | Z (pu) | Y/2 (pu) | R (pu) | L (pu) | C/2 (pu) |
|---|---|---|---|---|---|---|
| 1-2 | 120 | 0.01363+j0.10375 | j0.07852 | 0.01363 | 0.00033 | 0.00025 |
| 1-5 | 250 | 0.02788+j0.21423 | j0.16433 | 0.02788 | 0.00068 | 0.00052 |
| 5-2 | 175 | 0.01975+j0.15085 | j0.11468 | 0.01975 | 0.00048 | 0.00037 |
| 2-4 | 180 | 0.02030+j0.15511 | j0.11798 | 0.02030 | 0.00049 | 0.00038 |
| 2-3 | 200 | 0.02249+j0.17211 | j0.13118 | 0.02249 | 0.00055 | 0.00042 |
| 4-3 | 250 | 0.02788+j0.21423 | j0.16433 | 0.02788 | 0.00068 | 0.00052 |
| 5-4 | 100 | 0.01138+j0.08653 | j0.06541 | 0.01138 | 0.00028 | 0.00021 |
| $Z_{base}$= 484 Ω and $Y_{base}$=0.00207 S | | | | | | |

# 6 Grid-connected voltage source converter

The configuration of the grid-connected voltage source converter detailed in this section is a two-level converter. For simplicity purposes the following control scheme has been chosen.

The control system of the converter is depicted in Fig. 21. Which is comprised by the phase-locked loop (PLL), inner and outer controller. Notice that the outer control loop has been simplified, the active and reactive power references have been substituted by constant values for the reference currents. This is mainly done to reduce the complexity of the control system.

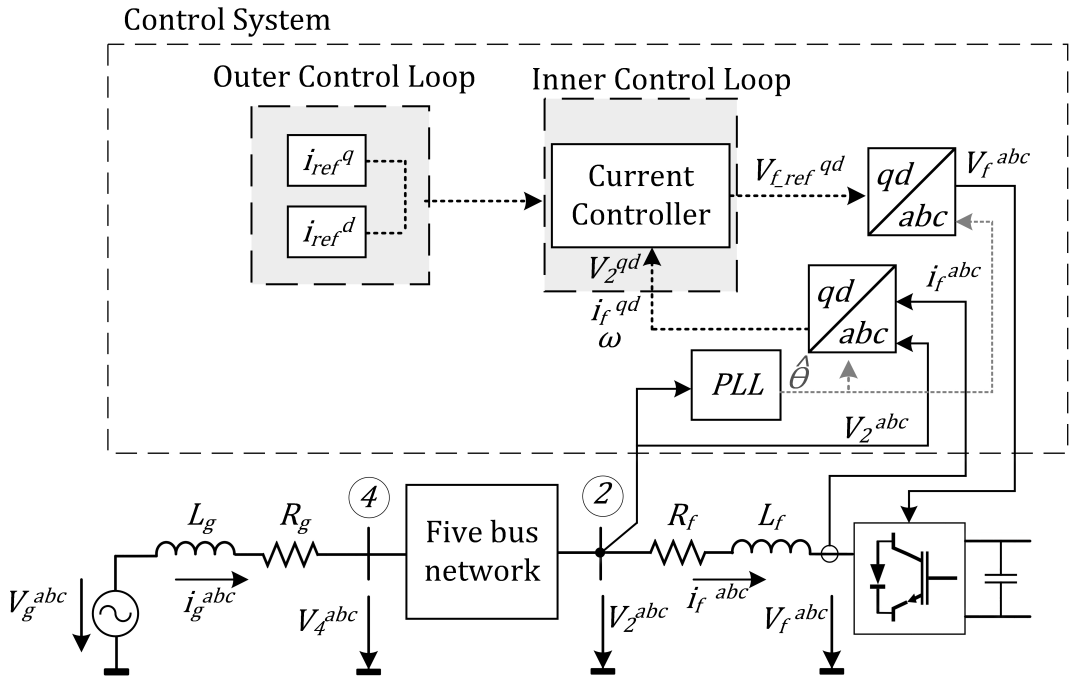


Figure 21: Grid-connected converter control system

## 6.1 Current control loop

The current control loop is the essential controller of the VSC converter, it regulates the current flowing trough the converter towards the grid by generating the proper voltage reference. The current control used in this thesis is based on the decoupled control, this allows the independent control of the active and reactive power. The decoupling is obtained when the PLL is adequately oriented, therefore, the voltage $d$ component is zero.

In order to obtain the constants of the proportional integral (PI) controller $K_{il}(s)$ in the current loop, the following expression can be derived. Applying Kirchhoff's voltage law between the converter and the bus 2 of Fig. 21 in the $s$-domain, then:

$$\mathbf{V_f^{qd}} = \mathbf{V_2^{qd}} - (R_f + sL_f)\,\mathbf{i_f^{qd}} + \omega L_f\,\mathbf{i_f^{dq}} \tag{6.1}$$

Obtaining the relationship of inputs and outputs of the block diagram of Fig. 22, the following

expression is derived:

$$\mathbf{V_f^{qd}} = \mathbf{V_2^{qd}} - K_{il}\left(\mathbf{i_{ref}^{qd}} - \mathbf{i_f^{qd}}\right) + \omega L_f\, \mathbf{i_f^{dq}} \tag{6.2}$$

By comparing (6.1) with (6.2), the PI $K_{il}(s)$ constants can be obtained, where $K_{il}(s) = K_{p\_il} + K_{i\_il}/s$ and the gains are $K_{p\_il} = \frac{L_f}{\tau_{il}}$ and $K_{i\_il} = \frac{R_f}{\tau_{il}}$[27]. The $\tau_{il}$ is the current control loop time constant. The gains values can be found in Table 4.

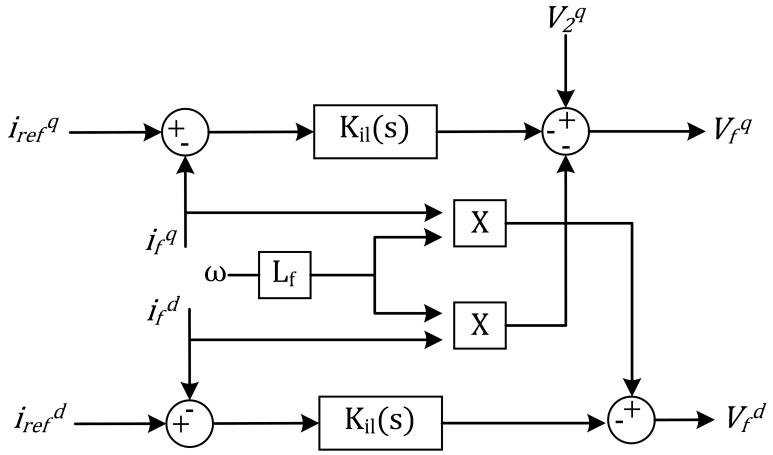


Figure 22: Block diagram of the current loop

## 6.2 Phase-locked loop

The phase-locked loop (PLL) is a tracking system that determines the phase angle and the angular velocity of the electrical network [28]. A three-phase PLL consists in a closed loop controller which tracks the angular velocity of the network by setting the voltage $d$ component to zero. The outputs of the controller are the estimated angular velocity $\hat{\omega}$ of the electrical grid and the integration of this signal provides the estimated grid angle $\hat{\theta}$.

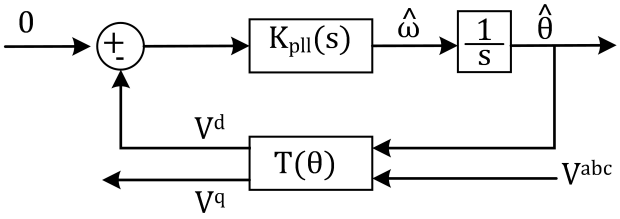


Figure 23: Block diagram of the PLL

where the controller $K_{pll} = K_{p\_pll} + K_{i\_pll}/s$. The proportional and integral gains have been tuned according to [28]. The gains values for the PLL can be found in Table 4.

## 6.3 Linear model of the system

The control loops of the VSC converter and the transformation effect introduced by the transformation matrix $T(\theta)$ are shown in the block diagram of Fig. 24. The linear model is comprised by the VSC converter, the five bus network and the equivalent network. The model becomes a small signal model because the model of the VSC converter is linearized.

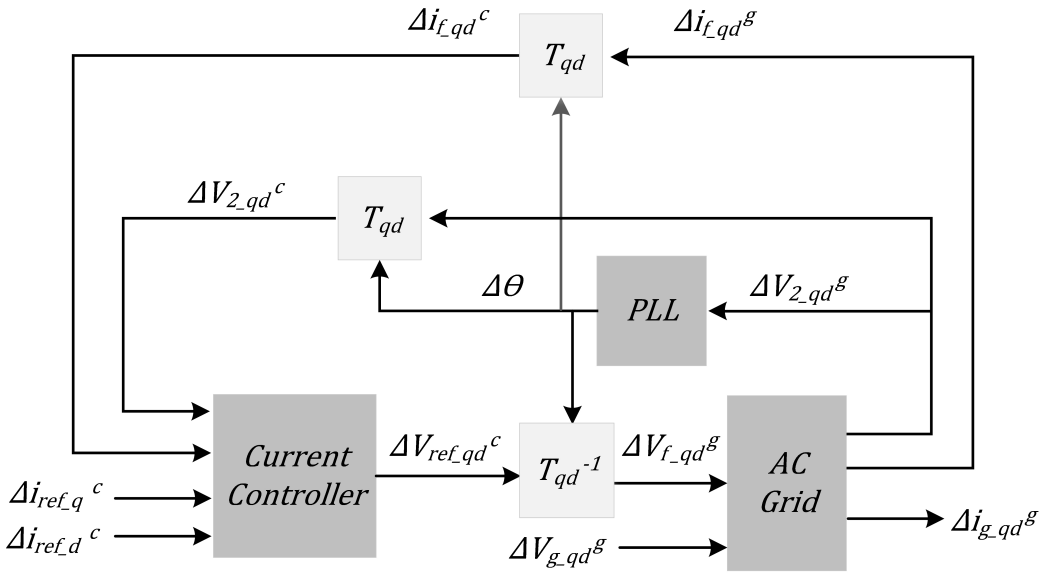


Figure 24: Block diagram of the linear model

The blocks $T_{qd}$ and $T_{qd}^{-1}$ are respectively the linearized transformation matrix $T(\Delta\theta)$ and the linearized inverse transformation matrix $T(\Delta\theta)^{-1}$. These blocks model the rotation effect of the transformation matrix. The matrix $T_{qd}$ is given by the following expression [11]:

$$\mathbf{T_{qd}} = \begin{bmatrix} \cos(\Delta\theta_0) & -\sin(\Delta\theta_0) & -\sin(\Delta\theta_0)\,\Delta x^g_{q0} - \cos(\Delta\theta_0)\,\Delta x^g_{d0} \\ \sin(\Delta\theta_0) & \cos(\Delta\theta_0) & \cos(\Delta\theta_0)\,\Delta x^g_{q0} - \sin(\Delta\theta_0)\,\Delta x^g_{d0} \end{bmatrix} \tag{6.3}$$

Notice that the variables in the block diagram have superscripts, where the superscript "$c$" stands for *converter* and the superscript "$g$" stands for *grid*. This two distinctions are important, because the variables work at different references. And choosing the proper variables at the proper reference is key to obtain the correct transformed variables. In Fig. 25 is shown the effect of the reference in the rotation of the variables, moving from the grid reference to the converter reference and conversely.

Where $\Delta\theta_1$ and $\Delta\theta_2$ are:

$$\Delta\theta_1 = \hat{\theta} - \theta_g \tag{6.4}$$

$$\Delta\theta_2 = \theta_g - \hat{\theta} \tag{6.5}$$

As it can be seen in Fig.25, there are two paths for going from the converter reference to the grid reference and both are equivalent. The inverse rotation $R^{-1}(\Delta\theta_1)$ allows to work with only one

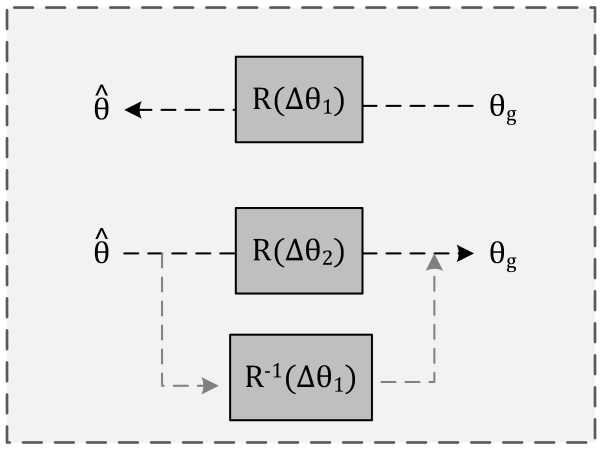


Figure 25: Reference frames

angle in the system. This is the main reason why $T_{qd}^{-1}$ is applied in the block diagram of Fig. 24, where $T_{qd}^{-1}$ is given by [11]:

$$\mathbf{T_{qd}^{-1}} = \begin{bmatrix} \cos(\Delta\theta_0) & \sin(\Delta\theta_0) & -\sin(\Delta\theta_0)\,\Delta x_{q0}^c + \cos(\Delta\theta_0)\,\Delta x_{d0}^c \\ -\sin(\Delta\theta_0) & \cos(\Delta\theta_0) & -\cos(\Delta\theta_0)\,\Delta x_{q0}^c - \sin(\Delta\theta_0)\,\Delta x_{d0}^c \end{bmatrix} \tag{6.6}$$

In Fig. 24 the block named "AC grid" is the SS model of the five bus network plus the equivalent network and the filter impedance of the VSC converter. Recall that the sense for the currents entering every node or bus is considered as positive when the SS model of the five bus network was derived in (3.69) and (3.70). Now that the VSC converter is connected to the bus 2 of the network the sense of the current $i_{2qd}$ at bus 2 is the opposite, it is not longer entering the system but leaving it towards the converter. This change in signs needs to be considered for the proper modelling of the system.

The filter impedance $Z_f$ of the grid-connected VSC converter needs to be modelled. The SS model of the filter impedance is similar to the one of the equivalent network given in (3.73), considering that the current $i_{2qd}$ flows from bus 2 to the terminals of the grid-connected VSC converter. Finally, the SS model of the control loops is derived to complete the linear model of the system and can be found in Appendix 7.8.

## 6.4 Validation of the VSC converter linear model

For the validation of the VSC converter linear model in time-domain, a non-linear model is created similar to the one shown in Figure 21. In order to validate properly the VSC converter linear model, the VSC converter is firstly connected only with an equivalent network and later it is connected to the five bus network. Table 4 details the parameters regarding the equivalent network and the VSC converter. Note that the unit of the variables is in pu. The base values are given in Section 5.

Table 4: Equivalent network and VSC converter parameters

| Parameter | Symbol | Value | Units |
|---|---|---|---|
| Equivalent network power | $S_g$ | 250 | MVA |
| Equivalent network voltage | $V_g$ | 220 | kV |
| Short circuit current | $SCC$ | 10 | |
| Grid X/R ratio | | 10 | |
| Resistance | $R_g$ | 0.0080 | pu |
| Inductance | $L_g$ | $2.5338 \times 10^{-4}$ | pu |
| Converter filter resistance | $R_f$ | 0.0022 | pu |
| Converter filter inductance | $L_f$ | $0.685 \times 10^{-3}$ | pu |
| Current control loop time constant | $\tau_{il}$ | 10 | ms |
| Current control loop proportional gain | $K_{p\_il}$ | 0.0685 | |
| Current control loop integral gain | $K_{i\_il}$ | 0.22 | |
| PLL time constant | $\tau_{PLL}$ | 12.50 | ms |
| PLL proportional gain | $K_{p\_PLL}$ | 160 | |
| PLL integral gain | $K_{i\_PLL}$ | 12800 | |

### 6.4.1 VSC converter connected to an equivalent network

In Fig. 26, it is shown the VSC converter connected to the equivalent network with a resistance $R_g$ and and inductance $L_g$. The current in the system flows from the voltage source $V_g{}^{abc}$ to the VSC converter.

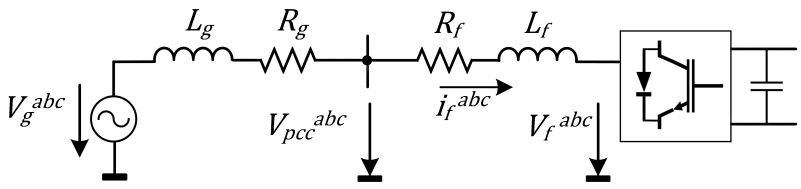


Figure 26: VSC converter connected to an equivalent network

To validate the non-linear model with the linear model, a small step is introduced in the current reference $i_{ref\_qd}$ at the time instant $t = 2\,\text{s}$. The following figures show the effect of the step on the variables of the converter. Fig. 27 shows the step in the voltage reference $V^c_{ref\_q}$ of the converter and Fig. 28 shows $\Delta\theta = \hat{\theta} - \theta_g$, where $\theta_g$ is the grid angle.

As expected, both models match properly. This indicates that the linear model is proper linearized and validated. The validation procedure is easier with a small system than a large one. As it is will be shown in Section 6.4.2, the five bus network introduces some slight variations in the response of the signals when a step occurs in the system and this may lead to believe that the validation is not correct.

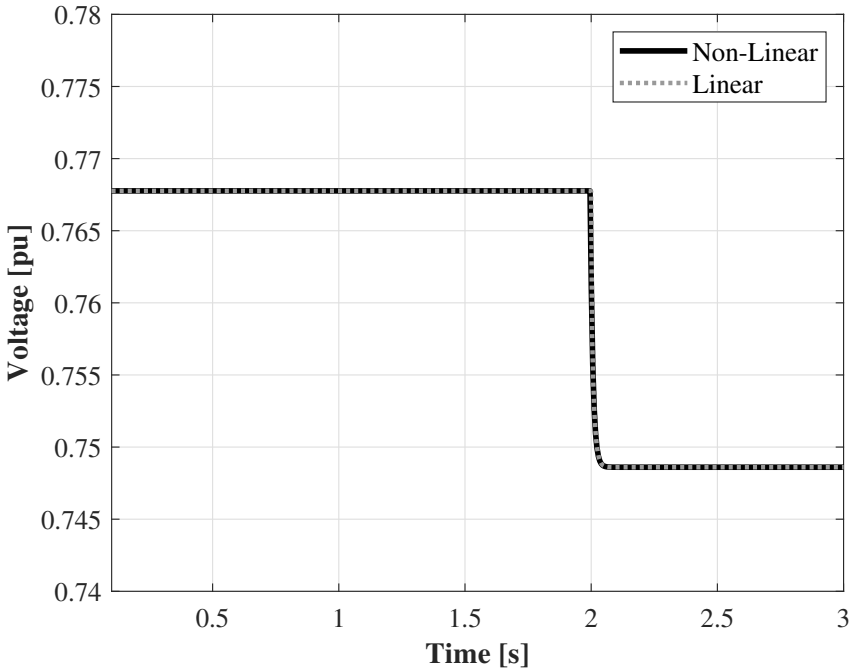


Figure 27: Small perturbation in the voltage reference $V^c_{ref\_q}$ of the converter

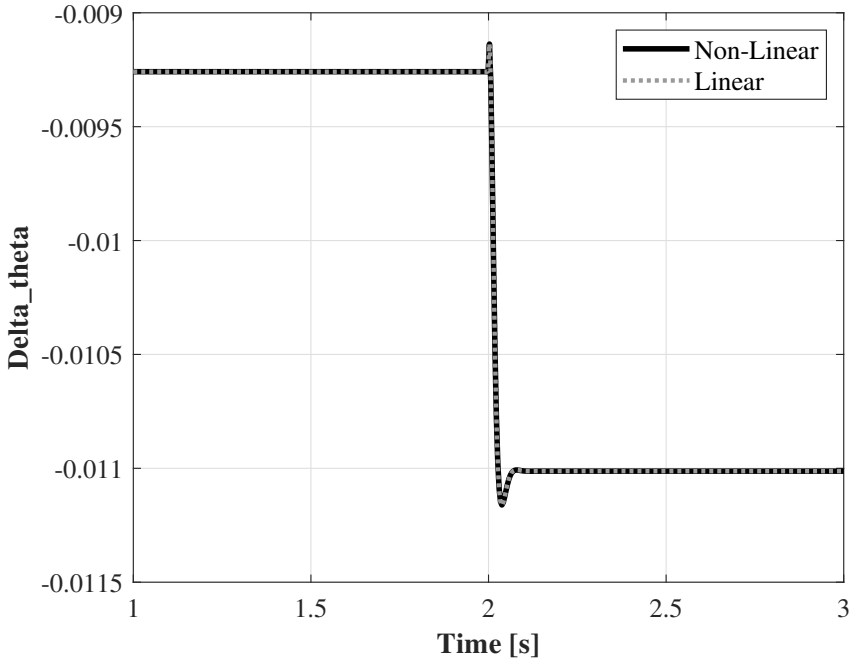


Figure 28: Difference between the estimated angle $\hat{\theta}$ and the grid angle $\theta_g$

### 6.4.2 VSC converter connected to the five bus network

The VSC converter is now connected with the five bus network and the equivalent network. The step in the current reference is applied again and the same variables are plotted as before.

In the figure below, it can be seen that the large power network introduces significant oscillations whenever a change in the network occurs. Consider that the network has a considerable amount of capacitive and inductive load due to the power lines. However the linear model follows exactly the non-linear model in the first milliseconds after the step is introduced and then it wanders slightly, but the steady state response match properly.

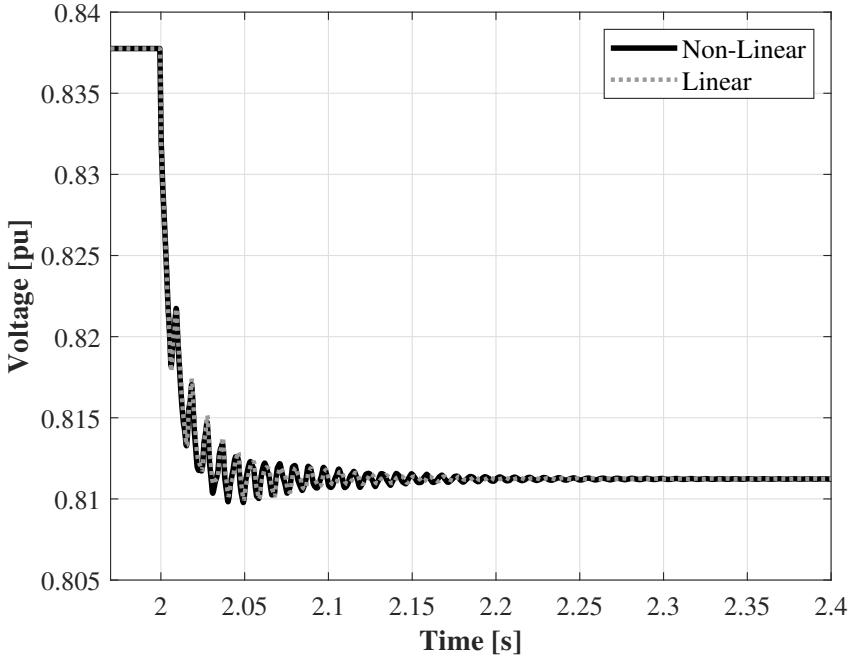


Figure 29: Small perturbation in the voltage reference $V^c_{ref\_q}$ of the converter

In Appendix 7.9 can be found more figures about the validation of the VSC converter.

# 7 Main findings

## 7.1 Short circuit ratio variation

The short circuit ratio of the equivalent network has been varied in order to study the stability of the system and see its behaviour under these conditions. Consider that the power lines that comprised the five bus network are considerably long and reducing the SCR of the equivalent network to smaller values would make the network weaker and the control of the VSC converter less accurate and prone to unstable conditions [8].

For simulation purposes, it is considered that the VSC converter is injecting $P_c = 0.80\,\text{pu}$ and $Q_c = 0.40\,\text{pu}$ and when the step is applied the power is stepped up to a $P_c = 0.88\,\text{pu}$ and $Q_c = 0.48\,\text{pu}$. Bear in mind that in this thesis, the outer control loop of the system is comprised by the current references $i_{ref\_qd}$, therefore, it is assumed that the the current reference "$q$" component is equal to the active power $P_c$ injection. And the current reference $d$ component is equal to the reactive power $Q_c$ injection. This is a very strong assumption, because it neglects the dynamics of the outer control loop due to the change in the voltage at the PCC whenever the conditions of the system change. Note that the unit of the variables is in pu. The base values are given in Section 5.

The figures below show the eigenvalues and the singular values of the system when the SCR is varied. It can be observed in Fig 30, that the poles of the system move progressively to the right half plane (RHP) as the SCR decreases. On the other hand, in Fig 31 peaks of resonance appear in the sub-synchronous region as the SCR decreases. Notice that for every signal the first peak appears in the frequency range of $[1 - 100]\,\text{Hz}$, the second peak in the range of $[100 - 200]\,\text{Hz}$ and then it comes a group of peaks in the range of $[300 - 1000]\,\text{Hz}$.

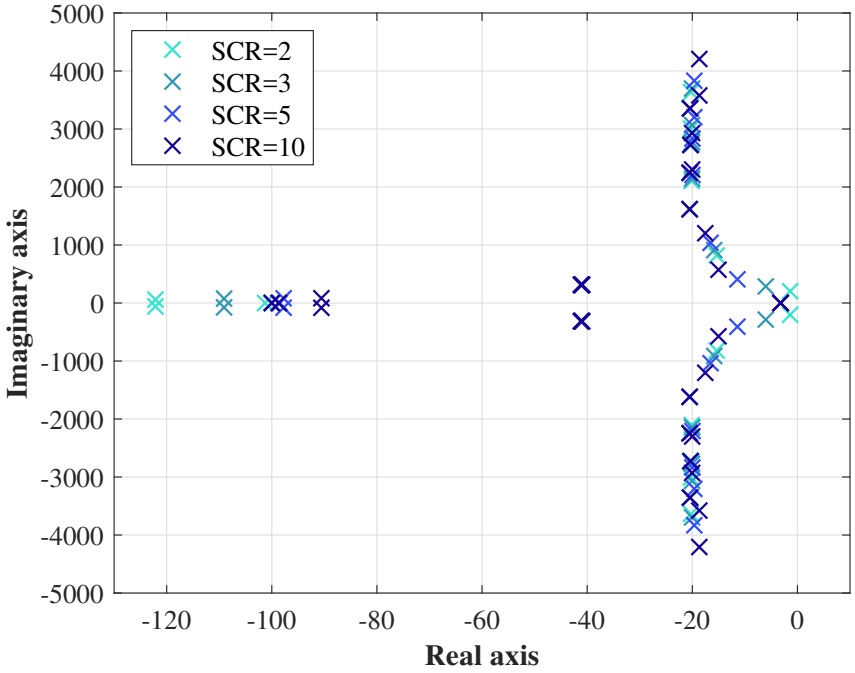


Figure 30: Eigenvalues of the system at different SCRs

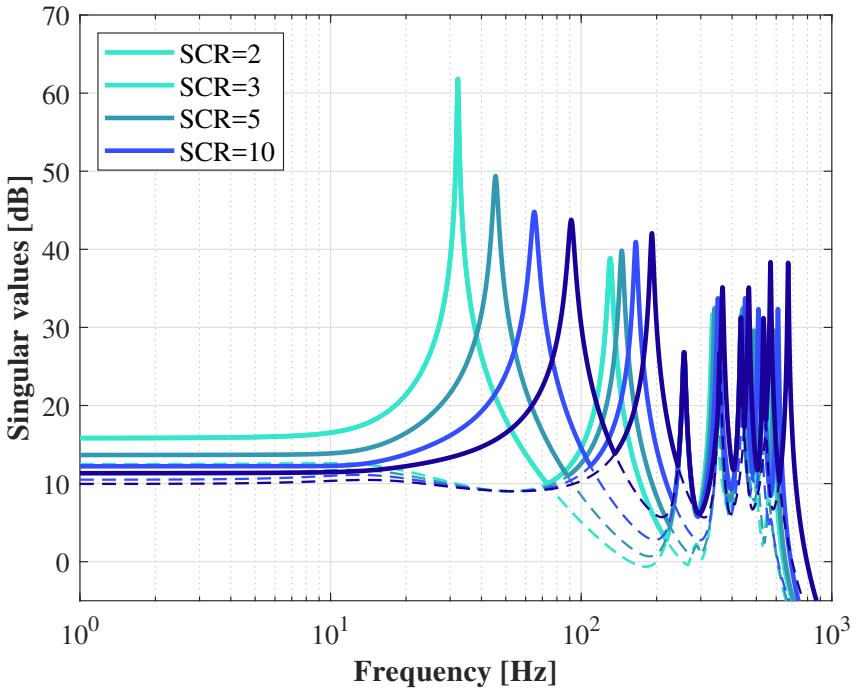


Figure 31: Singular values of the system at different SCRs

## 7.2 Power line outage

The power line 2-4 of the five bus network has been removed in order to analyze the stability of the system at different SCR values. Realize that a loss of power lines can occur in real power systems at any time and it is important to study the behaviour of the system under such conditions. As it can be observed in Fig. 32, there is a pair of poles that are located in the RHP when the SCR $= 2$. To be exactly, this pair of poles are located in the points $\lambda_{1,2} = 1.8461 \pm \text{j}214.9894$.

The singular values plot for different SCRs is shown in Fig. 33, note the graph at a SCR $= 2$ has a resonance peak at a sub-synchronous frequency of 34 Hz. Moreover, there is a second resonance peak at a sub-synchronous frequency of 47 Hz when the SCR $= 3$, close to the synchronous frequency of the grid. However, these results are similar to the ones obtained in Fig. 31.

The time response for the $V^c_{ref\_q}$ and the $i^c_{f\_q}$ at a SCR $= 2$ is shown in Fig. 34 and Fig. 35, respectively. Notice that the linear model becomes unstable when the step occurs at the time instant $t = 2\,\text{s}$. However, the non-linear model remains stable under the same conditions. This result is interesting because it shows that the linear model is not valid for this point of operation. There are certain nonlinearities under these operation conditions that are not captured properly by the linear model. This would require a more thorough study of the linear and non-linear model. Something to bear in mind is that the amount of apparent power $S_c$ that is being injected when the step occurs is 1 pu.

It is important to realize that the loss of a power line changes drastically the topology of the network and its characteristics. Also, the power flow needs to be redefined based on these changes and one can expect new imposed power transfer capabilities in the system.

Moreover, it has been remarked previously the amount of active and reactive power that is being

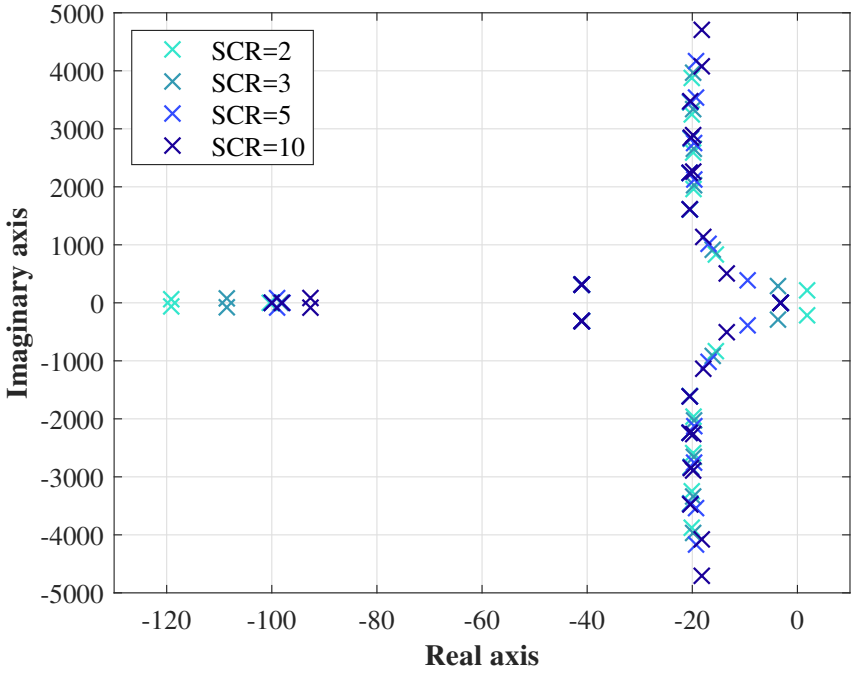


Figure 32: Eigenvalues for the system without line 2-4

injected into the network. Now, it is assessed the effect of changing the amount of reactive power from $Q_c = 0.40\,\text{pu}$ to $Q_c = 0.20\,\text{pu}$ before the step and then stepping up $Q_c = 0.28\,\text{pu}$ at the time instant $t = 2\,\text{s}$. The $P_c$ and the SCR=2 is kept the same.

The eigenvalues plot shown in Fig. 37 shows that the pair of poles that were unstable in Fig. 32 became stable just by changing the amount of $Q_c$ injected. The VSC converter would need to adjust to the new conditions of the network in order to avoid an unstable operation. This could be an example of the power limitations imposed by the loss of a power line in a given network.

However, due to the proximity of the pair of poles to the RHP oscillations can be expected, as it is shown in Fig. 38 where the voltage $V^c_{ref\_q}$ of the converter is depicted. Notice that the resonance peak in Fig 36 is the same in position as in Fig 33, but different in magnitudes. The resonance peak is still present in the sub-synchronous region, but with a lower magnitude. Therefore, the SCR variation affects the magnitude in the singular values plot.

The results obtained here lead to a sensitivity analysis of the VSC converter for different power operations, which is addressed in Section 7.3.

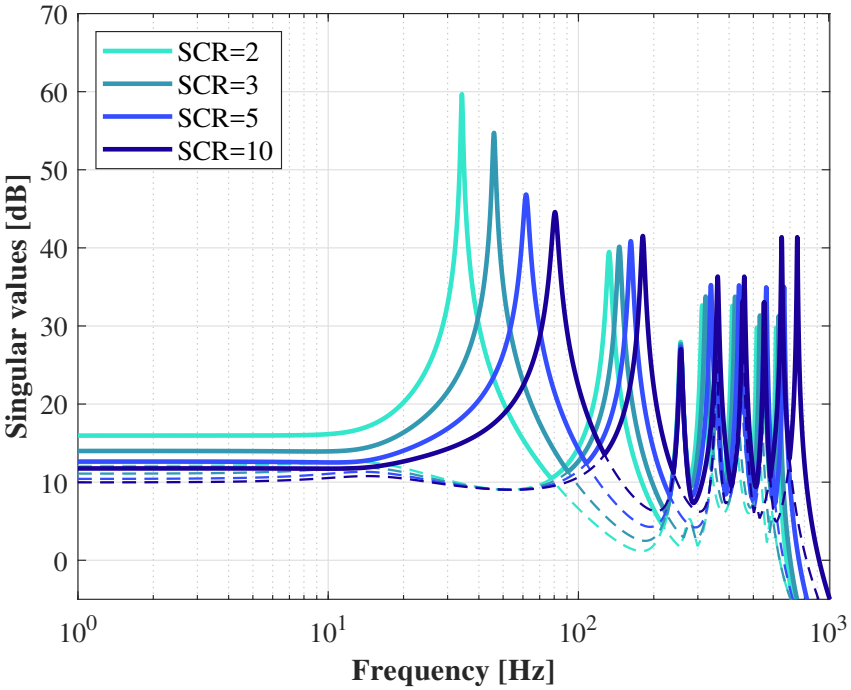


Figure 33: Singular values for the system without line 2-4

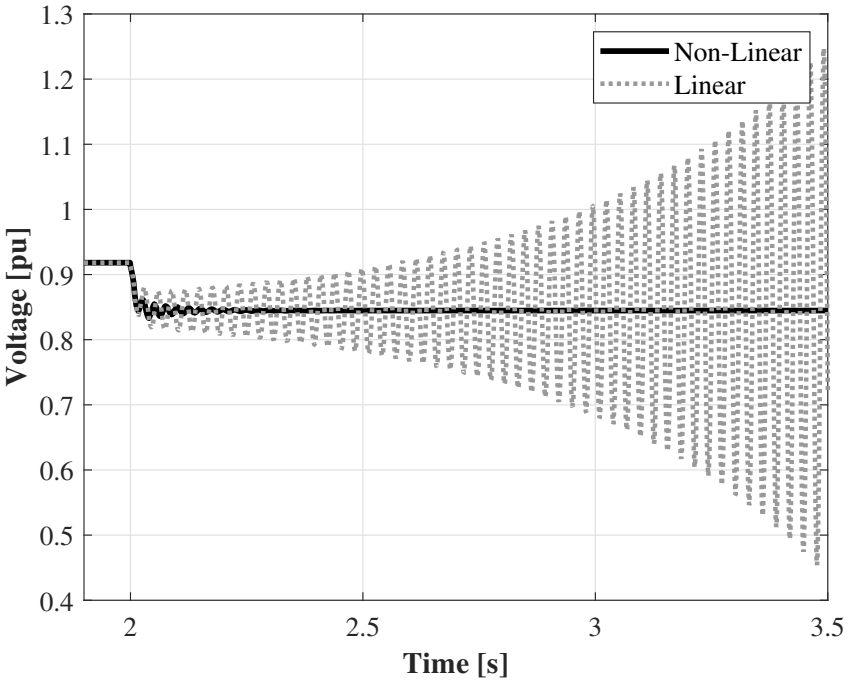


Figure 34: Voltage reference $V^c_{ref\_q}$

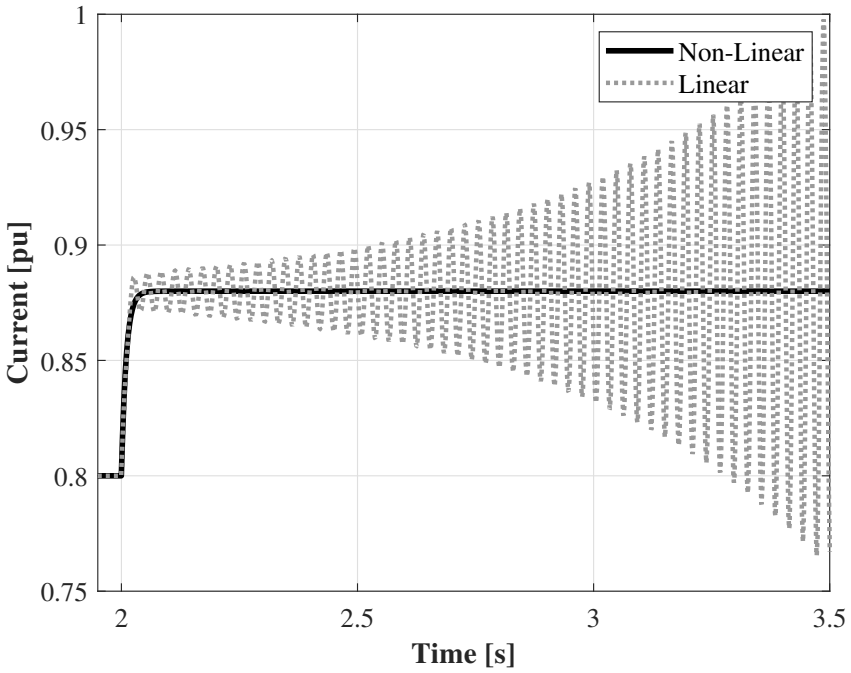


Figure 35: Current of the converter $i^c_{f\_q}$

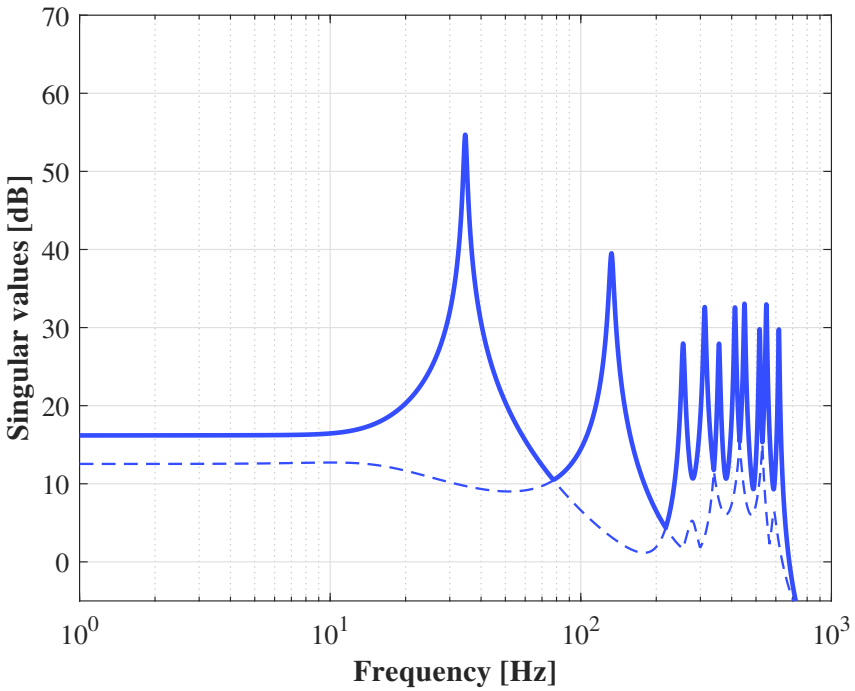


Figure 36: Singular values at SCR=2, $P_c = 0.80\,\text{pu}$ and $Q_c = 0.2\,\text{pu}$

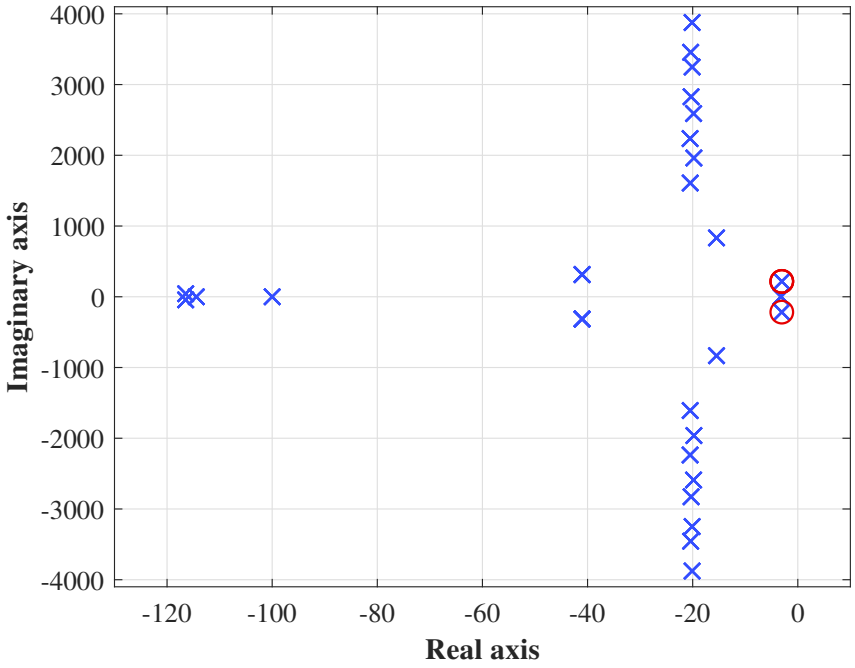


Figure 37: Eigenvalues at SCR=2, $P_c = 0.80\,\text{pu}$ and $Q_c = 0.20\,\text{pu}$

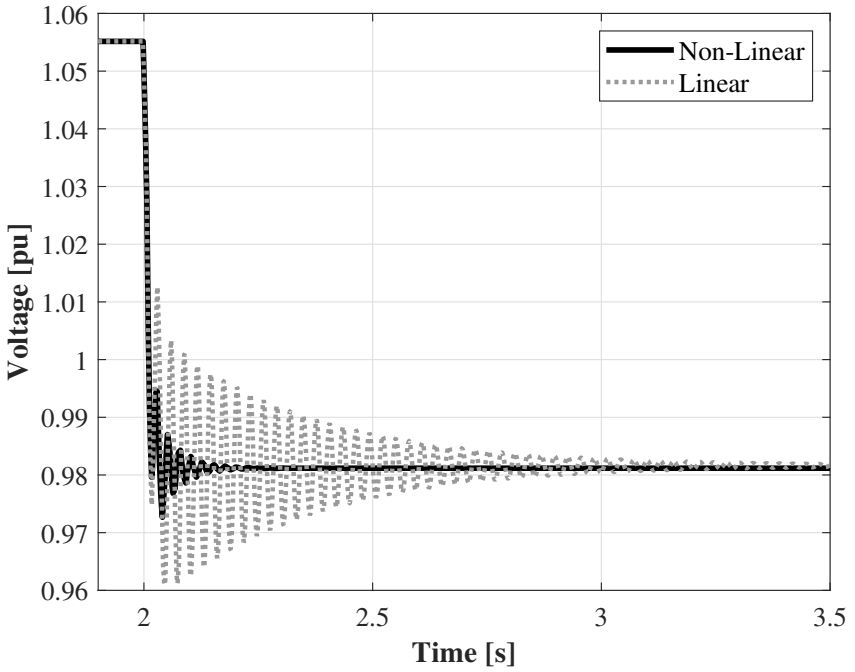


Figure 38: Voltage reference $V^c_{ref\_q}$ at SCR=2, $P_c = 0.88\,\text{pu}$ and $Q_c = 0.28\,\text{pu}$

## 7.3 Sensitivity analysis: power variation

The active and reactive power transfer capabilities of the VSC converter has limits that need to be considered to ensure a proper operation of the system. Consider that the power line outage introduced in Section 7.3 is still present for the simulations here described.

It would be interesting to study the effect of the power variation on the system, if the active power is varied in the intervals of $[-1 \leq P_c \leq 1]\,\mathrm{pu}$. The negative value of active power means that the converter is absorbing power and the positive value means that is injecting power. The well known expression for the apparent power $S_c$ allows to determine the reactive power $Q_c$. Consider that the VSC converter is injecting or absorbing $S_c = 1\,\mathrm{pu}$.

Where $S_c$ is:

$$S_c{}^2 = P_c{}^2 + Q_c{}^2$$

And solving for $Q_c$, it is obtained :

$$Q_c = \sqrt{1 - P_c{}^2}$$

As it was demonstrated before, one can expect stable operation of the system under a SCR $= 5$, therefore, the chosen SCR for the sensitivity analysis is 5.

Fig. 39 shows the poles variation of the system when the active power ranges from -1 to 1 pu with sampling intervals of 0.2 pu. The colours range goes from darker to lighter colours.

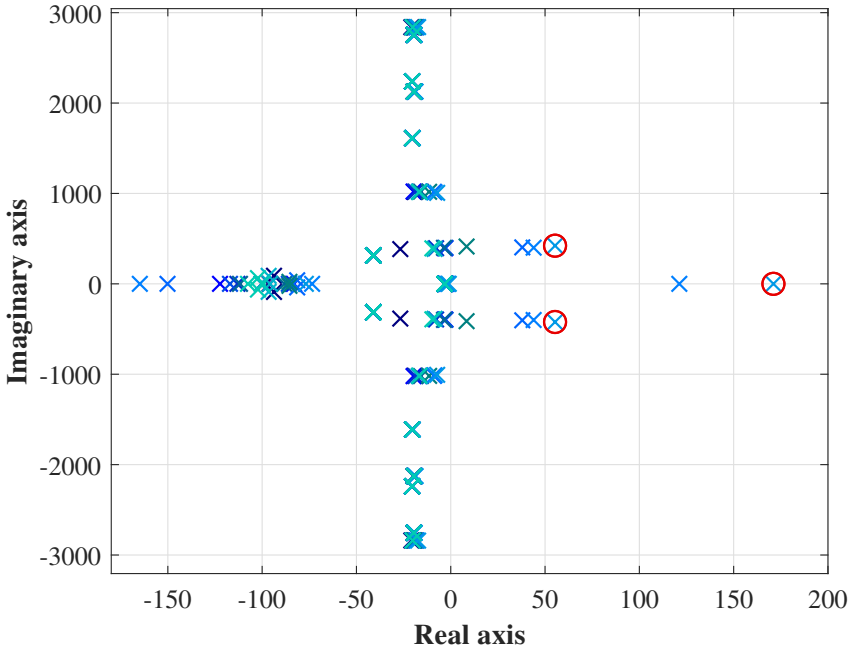


Figure 39: Eigenvalues for the sensitivity analysis

Notice that in Fig. 39 there are three encircled poles, these correspond to the scenario where the VSC converter is injecting $P_c = 0.6\,\mathrm{pu}$ and $Q_c = 0.8\,\mathrm{pu}$. Making a participation factor modal analysis of the system for this scenario, it is discovered that the unstable poles belong to the PLL.

The participation factor modal analysis allows to study the stability of a given system. The participation factor is a scalar value in the range of 0 to 1, that determines the degree of the system parameters influence on the formation of oscillations mode for linear systems [29]. In Appendix 7.10, it is shown the modal parameters and participation factors diagram for the example here described.

Fig. 40 shows the singular values of this scenario. It can be observed that the magnitude is around 22 dB for the range of frequencies of [1-100] Hz. This is an abnormal behaviour of the system if compared to Fig. 31 or Fig. 33 . There is also a small resonance at frequency of 65.62 Hz, which is above the synchronous frequency of the system. There is not any sub-synchronous resonance of high magnitude in the system, except for the slight increased magnitude in the range of [1-100] Hz.

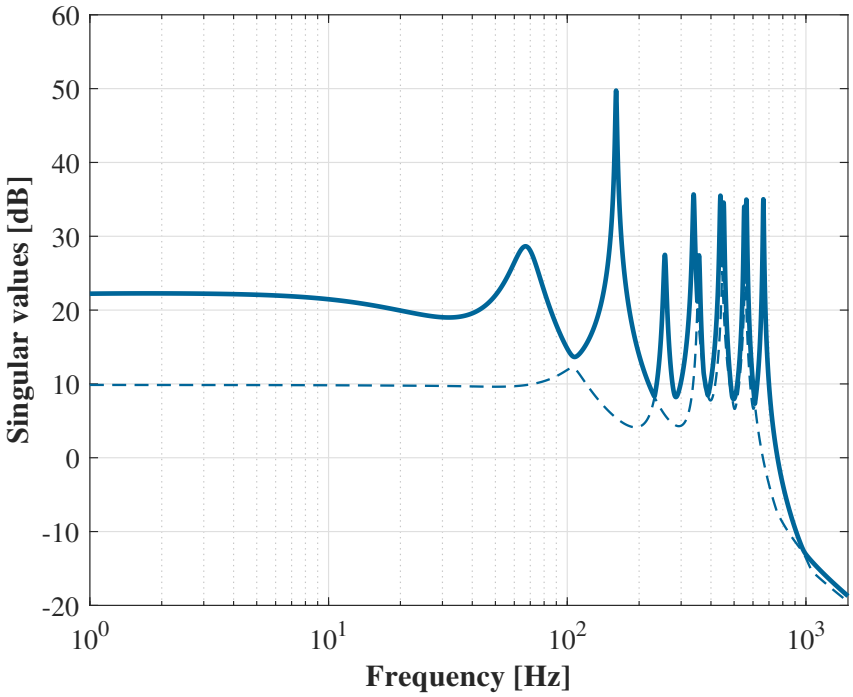


Figure 40: Singular values for the sensitivity analysis at $P_c = 0.6\,\mathrm{pu}$ and $Q_c = 0.8\,\mathrm{pu}$.

In Fig. 41 it is shown the response in time for the voltage of the converter $V^c_{ref\_q}$, the non-linear model of the system oscillates and the linear model of the system becomes unstable when the step occurs at the time instant $t = 2\,\mathrm{s}$. This is an interesting result, because it shows that the non-linear model is close to instability. On the other hand, the linear model being an approximation of the non-linear model is more prone to the instabilities becoming unstable. The other variables of the VSC converter follow a similar behaviour.

As it can be seen, there are power transfer capabilities that need be considered for stable operations regardless of the strength of the equivalent network. Reactive power is bounded by the AC terminal voltage [30], in order to keep the proper voltage drop limits inside the network.

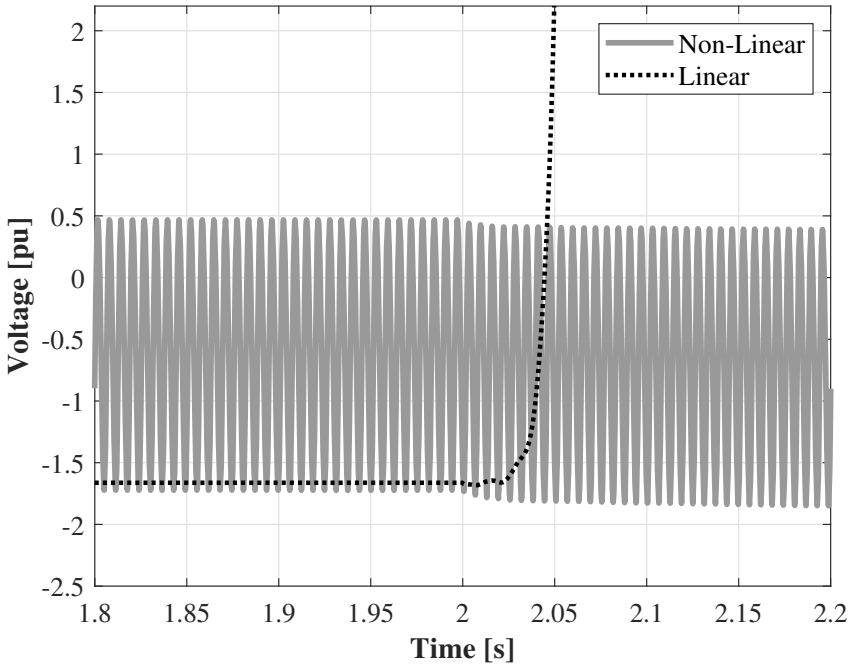


Figure 41: Voltage reference $V^c_{ref\_q}$ at $P_c = 0.6\,\text{pu}$ and $Q_c = 0.8\,\text{pu}$

## 7.4 More on power line outage

Previously it was shown the effect of the disconnection of a power line on the system. It would be interesting to see how the system behaves when different lines are disconnected. The power line 2-4 was disconnected before, there was not any particular reason for choosing that line, since the main goal was to asses how the system would behave under the new topology of the network.

Now, the eigenvalues and singular values for the system are plotted by disconnecting one different line of the system per simulation. Consider that the lines connected to bus 1 and bus 3 are in series, therefore it means that if line 1-5 is disconnected so it is line 1-2. The same happens for lines 2-3 and line 4-3. The complete network is also plotted to have a reference for comparison. In Fig. 20 is shown the power system. The chosen SCR for these simulations is 5.

As it can be seen in the figures found in Appendix 7.11, depending on which line is disconnected the system has a different behaviour. Under certain network topologies the poles move more to the RHP. Similarly, the singular values show the same behaviour by moving more to the sub-synchronous frequencies. The legend in the figures specify which line is removed.

# Conclusions

Important conclusions can be derived from the modelling process applying the admittance matrix and state-space representation in the $qd0$-domain to power networks.

1. The admittance matrix model can be easily derived, the matrix relates the voltages and currents of a network. Also, it becomes easy to check for possible mistakes or errors. Moreover, the manipulation of the matrix is straightforward by means of simple algebraic operations which allows to add, remove or change any value of the matrix.

2. The state-space model becomes challenging when the size of the network and the amount of elements capable of storing energy (i.e. capacitive and inductive elements) increase, manipulation of the SS model once it has been created becomes difficult due to some dependent variables.

3. In terms of validation, the state-space model becomes easy to validate, normally it is done by means of a model created in SIMULINK. On the other hand, the admittance matrix model is challenging when validation is required because it should be expressed as a transfer function, which it is obtained by solving for the desired variables. And for large matrices with many inputs and outputs is difficult to solve for the proper variables. Although, since it is so easy to check that every element of the admittance matrix is correct, no validation is often required. The validation discussed in this point it is a validation in time, in this thesis the validations were performed in the $s$-domain, whenever the models were compared.

4. As it was previously stated in Section 2.3, the size of the matrix in the admittance matrix model can become an issue when the inverse matrix is required, because of the large amount of data present in the matrix. This is an important characteristic to be considered when modelling large power networks and this definitely makes the state-space representation as the only possible modelling technique under such cases.

5. Other advantage of state-space representation over the admittance matrix, is the property to obtain easily any particular output variable response of the system. On the contrary, the admittance matrix requires more mathematical procedures to obtain the same output variable.

Regarding the VSC converter and the strength of the network the following conclusions can be derived:

1. Two models of the system were presented and discussed, the non-linear model created in MATLAB-SIMULINK and the state-space linear model. Both models were validated in time, firstly by connecting the VSC converter with an equivalent network and secondly by connecting it with the five bus network and equivalent network.

2. The angle $\Delta\theta$ provided by the PLL in the linear model should be properly referenced in the network, otherwise it would introduce phase shifts in the signals of the linear model making the comparison with the non-linear model to mismatch.

3. As detailed in Section 7, the SCR variation in the equivalent network demonstrates that the

linear model losses accuracy when the SCR is low. The linear model of the system is not valid for some conditions of operation. Being the linear model an approximation of the non-linear model, there are some non-linearities that appeared under certain conditions of operation (low SCR values) that are not approximated by the linear model.

4. The active and reactive power transfer capabilities are to be considered depending on the SCR value, as it was demonstrated. Changes in the topology of a network along with a low SCR would make the system weaker.

5. The results obtained in this thesis show that weak AC grids would impact on the VSC converter control system making it prone to instabilities. This thesis does not address any control solution as some literature does, but attempts to show the behaviour and interactions of a VSC converter when connected to a large network.

### Suggestions for future research

This thesis is focused on two modelling techniques for power systems and on the interactions of a grid-connected VSC converter with an AC grid. Because of this, some simplifications were made in the control system regarding the outer control loop. The next step would be to consider the complete model of the outer control loop to have a more detailed model of the system. It would be interesting too, to include more than one VSC converter in the power system and study the interactions between converters and the AC grid.

Another topic that would be interesting to study are the causes why the linear model does not approximate properly the non-linear model under certain conditions of operation.

Finally, something that would be helpful and interesting to develop is a MATLAB function capable of generating the state-space model of a given system regardless of its size. Also, capable of making any modification just by providing or removing the proper input data. This would make the modelling procedure faster and less complicated, specially for large power systems.

# References


[1] CIGRE WG C4/B4.38, "Network Modelling for Harmonic Studies," 2019.

[2] M. E. Van Valkenburg, *Network Analysis*. Prentice-Hall, 1964.

[3] J. J. Grainger and W. D. Stevenson, *Power System Analysis*. New York: McGraw-Hill, internatio ed., 1994.

[4] D. V. Hertem, O. Gomis-Bellmunt, and J. Liang, *HVDC GRIDS : For Offshore and Supergrid of the Future*. Hoboken, New Jersey: Wiley-IEEE Press, 1 ed., 2016.

[5] H. W. Beaty and D. G. Fink, *Standard Handbook for Electrical Engineers*. McGraw-Hill, sixteenth ed., 2013.

[6] L. Zhang, L. Harnefors, and H. P. Nee, "Interconnection of two very weak AC systems by VSC-HVDC links using power-synchronization control," *IEEE Transactions on Power Systems*, vol. 26, no. 1, pp. 344–355, 2011.

[7] The Transmission and Distribution Committee of the IEEE Power Engineering, *IEEE Guide for Planning DC Links Terminating at AC Locations Having Low Short-Circuit Capacities*, vol. 1997. 1997.

[8] J. Khazaei, P. Idowu, A. Asrari, A. B. Shafaye, and L. Piyasinghe, "Review of HVDC control in weak AC grids," *Electric Power Systems Research*, vol. 162, no. February, pp. 194–206, 2018.

[9] J. Z. Zhou, H. Ding, S. Fan, Y. Zhang, and A. M. Gole, "Impact of Short-Circuit Ratio and Phase-Locked-Loop Parameters on the Small-Signal Behavior of a VSC-HVDC Converter," *IEEE Transactions on Power Delivery*, vol. 29, no. 5, pp. 2287–2296, 2014.

[10] L. Xu and L. Fan, "Impedance-Based Resonance Analysis in a VSC-HVDC System," *IEEE Transactions on Power Delivery*, vol. 28, no. 4, pp. 2209–2216, 2013.

[11] A. Egea-Alvarez, S. Fekriasl, F. Hassan, and O. Gomis-Bellmunt, "Advanced Vector Control for Voltage Source Converters Connected to Weak Grids," *IEEE Transactions on Power Systems*, vol. 30, no. 6, pp. 3072–3081, 2015.

[12] D. Wang, Y. Hou, and J. Hu, "Effect of AC voltage control on the stability of weak AC grid connected DFIG system," *Asia-Pacific Power and Energy Engineering Conference, APPEEC*, vol. 2016-Decem, no. 51277155, pp. 1528–1533, 2016.

[13] Y. Li, G. Tang, T. An, H. Pang, P. Wang, J. Yang, Y. Wu, and Z. He, "Power Compensation Control for Interconnection of Weak Power Systems by VSC-HVDC," *IEEE Transactions on Power Delivery*, vol. 32, no. 4, pp. 1964–1974, 2017.

[14] Y. Huang, X. Yuan, J. Hu, and P. Zhou, "Modeling of VSC Connected to Weak Grid for Stability Analysis of DC-Link Voltage Control," *IEEE Journal of Emerging and Selected Topics in Power Electronics*, vol. 3, no. 4, pp. 1193–1204, 2015.

[15] C. Guo, W. Liu, C. Zhao, and R. Iravani, "A Frequency-Based Synchronization Approach

for the VSC-HVDC Station Connected to a Weak AC Grid," *IEEE Transactions on Power Delivery*, vol. 32, no. 3, pp. 1460–1470, 2017.

[16] M. F. M. Arani and Y. A. R. I. Mohamed, "Analysis and Performance Enhancement of Vector-Controlled VSC in HVDC Links Connected to Very Weak Grids," *IEEE Transactions on Power Systems*, vol. 32, no. 1, pp. 684–693, 2017.

[17] L. Zhang, L. Harnefors, and H.-p. Nee, "Power-Synchronization Control of Grid-Connected Voltage-Source Converters," *IEEE Transactions on Power Systems*, vol. 25, no. 2, pp. 809–820, 2010.

[18] "Maplesoft - Software for Mathematics, Online Learning, Engineering."

[19] C. K. Alexander and M. N. O. Sadiku, *Fundamentals of Electric Circuits*. New York: McGraw-Hill, 5th ed., 2013.

[20] D. C. Lay, *Linear Algebra and its applications*. Pearson, 4th ed., 2012.

[21] H. Akagi, E. H. Watanabe, and M. Aredes, *Instantaneous Power Theory And Applications To Power Conditioning*. Wiley, 2007.

[22] A. Egea-Alvarez, A. Junyent-Ferré, and O. Gomis-Bellmunt, "Active and Reactive Power Control of Grid Connected Distributed Generation Systems," *Modeling and Control of Sustainable Power Systems: Towards Smarter and Greener Electric Grids*, pp. 47–81, 2012.

[23] W. S. Levine, *The Control Handbook: Control System Fundamentals*. CRC Press, 2010.

[24] MathWorks, "Eigenvalues and eigenvectors-MATLAB Documentation," 2013.

[25] MathWorks, "Singular values plot of dynamic system-MATLAB Documentation," 2015.

[26] S. Skogestad and I. Postlethwaite, *Multivariable feedback control: analysis and design*. New York: Wiley, 2007.

[27] L. Harnefors and H. P. Nee, "Model-Based Current Control of AC Machines Using the Internal Model Control Method," *IEEE Transactions on Industry Applications*, vol. 34, no. 1, pp. 133–141, 1998.

[28] S.-k. Chung, "A Phase Tracking System for Three Phase Utility Interface Inverters," *IEEE Transactions on Power Electronics*, vol. 15, no. 3, pp. 431–438, 2000.

[29] V. Konoval and R. Prytula, "Participation Factor in Modal Analysis of Power Systems Stability," no. 86, 2016.

[30] M. Imhof, *Voltage Source Converter Based HVDC-Modelling and Coordinated Control to Enhance Power System Stability*. No. 22914, 2015.

[31] P. Kundur, *Power System Stability and Sontrol*. McGraw-Hill Education, 1994.

[32] Red Eléctrica Española, "The Spanish Electricity System," p. 200, 2017.

# Appendices

## 7.5 Power line parameters calculation

### 7.5.1 Equivalent-pi parameters

Here it is detailed the calculation of the OHL parameters for the five bus network. Due to the topology of the network and the length of the lines, distributed parameters for the lines are considered.

The distributed parameters of a power line are represented by an equivalent-pi [3], shown in Fig. 42.

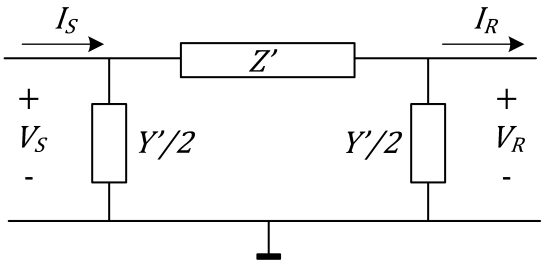


Figure 42: Equivalent-pi of a transmission power line

The subscript "$S$" and "$R$", stand for *sending* and *receving* ends, respectively.
Where $Z'$ and $Y'$ are:

$$Z' = \frac{Z \sinh(\gamma\ell)}{\gamma\ell} \qquad \frac{Y'}{2} = \frac{Y}{2}\frac{\tanh(\gamma\ell/2)}{(\gamma\ell/2)} \tag{7.1}$$

And $Z$ and $Y$ are :

$$Z = z\ell = (R + jX_L)\,\ell \qquad Y = y\ell = (G + jX_C)\ell \tag{7.2}$$

From (7.2), it can be appreciated the resistance $R$, the inductive reactance $X_L$, the capacitive reactance $X_C$ and the conductance $G$ of a transmission line of length $\ell$. However, the conductance $G$ is considered to be zero for all calculation purposes in this thesis.

The propagation constant $\gamma$ in (7.1), is given by the following expression:

$$\gamma = \sqrt{zy} \tag{7.3}$$

### 7.5.2 Inductance and capacitance of overhead power lines

Based on the information given in Table 2, the inductance and capacitance of the transmission lines can be calculated. The coordinates of the transmission lines are shown in Fig. 43.

The inductance is given by the following expression:

$$L = 0.2 \ln \frac{GMD}{GMR} \ \left[\text{mH/km}\right] \tag{7.4}$$

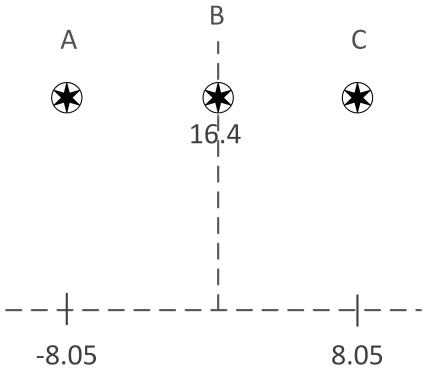


Figure 43: Transmission lines coordinates

And the capacitance:

$$C = \frac{1000}{18 \ln \frac{GMD}{r_{cond}}} \ \left[\mathrm{nF/km}\right] \tag{7.5}$$

where the geometric mean distance $GMD$ is:

$$GMD = \sqrt[3]{d_{AB}\, d_{BC}\, d_{CA}} \ \left[\mathrm{m}\right] \tag{7.6}$$

The $d$ term in (7.6) is the distance between conductors and the $r_{cond}$ term in (7.5) is the outer radius of the conductor. Previous equations are taken from [3].

Taking into account the data provided and the equations detailed previously, let us calculate the inductance and capacitance.

The $GMD$ of the transmission lines is :

$$GMD = \sqrt[3]{8.05 \times 8.05 \times 16.01} = 10.1424\,\mathrm{m} \tag{7.7}$$

The outer radius of the conductor and geometric mean radius are given in Table 2.

The inductance is:

$$L = 0.2 \ln \frac{10.1424}{12.757\,33 \times 10^{-3}} = 1.3357\,\mathrm{mH/km} \tag{7.8}$$

The conductance is:

$$C = \frac{1000}{18 \ln \frac{10.1424}{15.8115 \times 10^{-3}}} = 8.5950\,\mathrm{nF/km} \tag{7.9}$$

Once the inductance $L$ and capacitance $C$ are obtained, it is straight forward the calculation of the impedance $z$ and admittance $y$ of the equivalent-pi transmission line.

## 7.6 Thevenin equivalent

Here is described the Thevenin equivalent network, it is assumed a $X/R = 10$ and a variable SCC. In order to obtain the impedance of the equivalent network, it is assumed that the amount of active power capable of exchanging is 250 MVA.

The impedance $Z_{eqv}$ can be calculated as follows:

$$Z_{eqv} = \frac{V^2}{S_{eq}\, SCC} \frac{1}{Z_{base}} \ \text{[pu]} \tag{7.10}$$

The resistance $R_{eqv}$ and reactance $X_{eqv}$ are respectively the real and imaginary part of the impedance $Z_{eqv}$. Since $X/R = 10$ the following expression is obtained:

$$\begin{aligned} Z_{eqv} =& \sqrt{R_{eqv}^2 + X_{eqv}^2} \\ =& \sqrt{R_{eqv}^2 + \left(10 R_{eqv}\right)^2} \\ =& R_{eqv}\sqrt{101} \end{aligned} \tag{7.11}$$

Solving for $R_{eqv}$ of (7.11):

$$R_{eqv} = \frac{Z_{eqv}}{\sqrt{101}} \ \text{[pu]} \tag{7.12}$$

And $X_{eqv}$ is :

$$X_{eqv} = 10\frac{Z_{eqv}}{\sqrt{101}} \ \text{[pu]} \tag{7.13}$$

## 7.7 VSC converter filter parameters

The grid-connected converter parameters are given in Table 5. Data is taken from the Inelfe project, which is the interconnection link between Spain and France. Due to confidentiality reasons, only generic data is provided.

Notice that the power rate of the VSC converter and transformer do not match the ones previously defined for the five bus network. However, what it is important to obtain from the table is the filter resistance $R_f$ and inductance $L_f$.

Table 5: Converter and power transformer parameters

| Parameter | Symbol | Value | Units |
|---|---|---|---|
| Converter power | $S_c$ | $1 \times 10^9$ | VA |
| Arm inductance | $L_c$ | $50 \times 10^{-3}$ | H |
| Arm resistance | $R_c$ | $68.22 \times 10^{-3}$ | Ω |
| Number of cells | $n_c$ | 400 | |
| Cells capacitance | $C_c$ | $9.5 \times 10^{-3}$ | F |
| Transformer voltage ratio | $a$ | 333/400 | |
| Converter side voltage | $V_c$ | 333 | kV |
| Grid side voltage | $V_{grid}$ | 400 | kV |
| Transformer power | $S_t$ | $1.059 \times 10^9$ | VA |
| Resistance | $R_t$ | 0.00212 | pu |
| Reactance | $X_t$ | 0.18 | pu |

The mismatch in power is irrelevant, because the main purpose is to show the order of magnitude of the parameters. Consider also that the values are expressed in per unit.

First it should be determined the resistance and reactance of the transformer in its respective units. For doing so, the base impedance $Z_{base}$ needs to be determined, then:

$$Z_{base} = \frac{V_{base}^2}{S_{base}} = \frac{V_{grid}^2}{S_t} = \frac{(400 \times 10^3)^2}{1.059 \times 10^9} = 151.10\,\Omega \tag{7.14}$$

Multiplying $R_t$ and $X_t$ per $Z_{base}$, then:

$$R_t = 0.00212 \times Z_{base} = 0.32\,\Omega \tag{7.15}$$

and:

$$X_t = 0.18 \times Z_{base} = 27.20\,\Omega \tag{7.16}$$

Now it can be calculated the $R_f$ and $L_f$. Also, the arm inductance $L_c$ and resistance $R_c$ need to be referenced to the secondary side of the transformer, then:

$$R_f = R_t + a^2\frac{R_c}{2} = 0.32 + \left(\frac{330}{400}\right)^2 \times \left(\frac{68.22 \times 10^{-3}}{2}\right) = 0.343\,\Omega \tag{7.17}$$

and :

$$L_f = \frac{X_t}{w} + a^2\frac{L_c}{2} = \frac{27.20}{2\pi 50} + \left(\frac{330}{400}\right)^2 \times \left(\frac{50 \times 10^{-3}}{2}\right) = 0.104\,\Omega \tag{7.18}$$

Changing (7.17) and (7.18) into pu, then:

$$R_f = \frac{R_f}{Z_{base}} = 0.0022\,\text{pu} = 0.22\,\% \tag{7.19}$$

and:

$$L_f = \frac{L_f}{Z_{base}} = 0.685 \times 10^{-3}\,\text{pu} = 0.0685\,\% \tag{7.20}$$

## 7.8 Linear model of the system

The linear model of the system is properly described by means of the SS representation. For better understanding of the variables and developed equations below, the reader is referred to Figure 24.

### 7.8.1 The phase-locked loop

The state-space representation of the PLL is given by the following expression in matrix form:

$$\begin{aligned} \mathbf{A_{pll}} &= \begin{bmatrix} 0 & 0 \\ -k_{i\_pll} & 0 \end{bmatrix} \quad \mathbf{B_{pll}} = \begin{bmatrix} 1 \\ -k_{p\_pll} \end{bmatrix} \\ \mathbf{C_{pll}} &= \begin{bmatrix} 0 & 1 \end{bmatrix} \qquad\quad \mathbf{D_{pll}} = [0_{1x1}] \end{aligned} \tag{7.21}$$

where $\dot{\mathbf{x}}_{\mathbf{pll}} = \begin{bmatrix} \Phi & \hat{\theta} \end{bmatrix}^T$, $\mathbf{u_{pll}} = \begin{bmatrix} V_{2\_d}^c \end{bmatrix}$ and $\mathbf{y_{pll}} = \begin{bmatrix} \hat{\theta} \end{bmatrix}$.

### 7.8.2 The current control loop

The state-space representation of the current control loop is given by the following expression in matrix form:

$$\begin{aligned} \mathbf{A_{il}} &= [0_{2x4}] & \mathbf{B_{il}} &= \begin{bmatrix} 1 & 0 & -1 & 0 & 0 & 0 \\ 0 & 1 & 0 & -1 & 0 & 0 \end{bmatrix} \\ \mathbf{C_{il}} &= \begin{bmatrix} -k_{i\_il} & 0 \\ 0 & -k_{i\_il} \end{bmatrix} & \mathbf{D_{il}} &= \begin{bmatrix} -k_{p\_il} & 0 & k_{p\_il} & -\omega L_f & 1 & 0 \\ 0 & -k_{p\_il} & \omega L_f & k_{p\_il} & 0 & 1 \end{bmatrix} \end{aligned} \tag{7.22}$$

where $\dot{\mathbf{x}}_{\mathbf{il}} = \begin{bmatrix} i_{e\_q} & i_{e\_d} \end{bmatrix}^T$, $\mathbf{u_{il}} = \begin{bmatrix} i_{ref\_q} & i_{ref\_d} & i^c_{f\_q} & i^c_{f\_d} & V^c_{2\_q} & V^c_{2\_d} \end{bmatrix}^T$ and $\mathbf{y_{il}} = \begin{bmatrix} V^c_{ref\_q} & V^c_{ref\_d} \end{bmatrix}^T$.

### 7.8.3 Linearized transformation matrix

To be able to include the rotation effect of the Transformation Matrix $T(\theta)$ in the linear model, $T(\theta)$ needs to be linearized. Small signals are assumed and the non-linear model can be expressed in terms of Taylor's series expansion [31].

Rotation effect of the transformation matrix for the voltage $V_{2\_qd}$ at the Bus 2 , from the $abc$-domain to the $qd0$-domain:

$$\begin{aligned} \mathbf{A_{Tv}} &= [0_{1x1}] & \mathbf{B_{Tv}} &= [0_{1x3}] \\ \mathbf{C_{Tv}} &= [0_{2x1}] & \mathbf{D_{Tv}} &= \begin{bmatrix} \cos(\Delta\theta_0) & -\sin(\Delta\theta_0) & -\sin(\Delta\theta_0)\,\Delta V^g_{2\_q0} - \cos(\Delta\theta_0)\,\Delta V^g_{2\_d0} \\ \sin(\Delta\theta_0) & \cos(\Delta\theta_0) & \cos(\Delta\theta_0)\,\Delta V^g_{2\_q0} - \sin(\Delta\theta_0)\,\Delta V^g_{2\_d0} \end{bmatrix} \end{aligned} \tag{7.23}$$

where $\dot{\mathbf{x}}_{\mathbf{Tv}} = [0]^T$, $\mathbf{u_{Tv}} = \begin{bmatrix} V^g_{2\_q} & V^g_{2\_d} & \hat{\theta} \end{bmatrix}^T$ and $\mathbf{y_{Tv}} = \begin{bmatrix} {V^c}_{2\_q} & {V^c}_{2\_d} \end{bmatrix}^T$.

Rotation effect effect of the transformation matrix for the current of the converter $i_{f\_qd}$, from the $abc$-domain to the $qd0$-domain:

$$\begin{aligned} \mathbf{A_{Ti}} &= [0] & \mathbf{B_{Ti}} &= [0_{1x3}] \\ \mathbf{C_{Ti}} &= [0_{2x1}] & \mathbf{D_{Ti}} &= \begin{bmatrix} \cos(\Delta\theta_0) & -\sin(\Delta\theta_0) & -\sin(\Delta\theta_0)\,\Delta i^g_{f\_q0} - \cos(\Delta\theta_0)\,\Delta i^g_{f\_d0} \\ \sin(\Delta\theta_0) & \cos(\Delta\theta_0) & \cos(\Delta\theta_0)\,\Delta i^g_{f\_q0} - \sin(\Delta\theta_0)\,\Delta i^g_{f\_d0} \end{bmatrix} \end{aligned} \tag{7.24}$$

where $\dot{\mathbf{x}}_{\mathbf{Ti}} = [0]^T$, $\mathbf{u_{Ti}} = \begin{bmatrix} i^g_{f\_q} & i^g_{f\_d} & \hat{\theta} \end{bmatrix}^T$ and $\mathbf{y_{Ti}} = \begin{bmatrix} {i^c}_{f\_q} & {i^c}_{f\_d} \end{bmatrix}^T$.

Rotation effect effect of the transformation matrix for the voltage of the converter $V_{ref\_qd}$, from the $qd0$-domain to the $abc$-domain:

$$\begin{aligned} \mathbf{A_{iTv}} &= [0] & \mathbf{B_{iTv}} &= [0_{1x3}] \\ \mathbf{C_{iTv}} &= [0_{2x1}] & \mathbf{D_{iTv}} &= \begin{bmatrix} \cos(\Delta\theta_0) & \sin(\Delta\theta_0) & -\sin(\Delta\theta_0)\,\Delta V^c_{ref\_q0} + \cos(\Delta\theta_0)\,\Delta V^c_{ref\_d0} \\ -\sin(\Delta\theta_0) & \cos(\Delta\theta_0) & -\cos(\Delta\theta_0)\,\Delta V^c_{ref\_q0} - \sin(\Delta\theta_0)\,\Delta V^c_{ref\_d0} \end{bmatrix} \end{aligned} \tag{7.25}$$

where $\dot{\mathbf{x}}_{\mathbf{iTv}} = [0]^T$, $\mathbf{u_{iTv}} = \begin{bmatrix} {V^c}_{ref\_q} & {V^c}_{ref\_d} & \hat{\theta} \end{bmatrix}^T$ and $\mathbf{y_{iTv}} = \begin{bmatrix} V^g_{f\_q} & V^g_{f\_d} \end{bmatrix}^T$.

## 7.9 Figures of the validation of the VSC converter

Fig. 44 and Fig. 45 shows the validation of the VSC converter connected to the equivalent network.

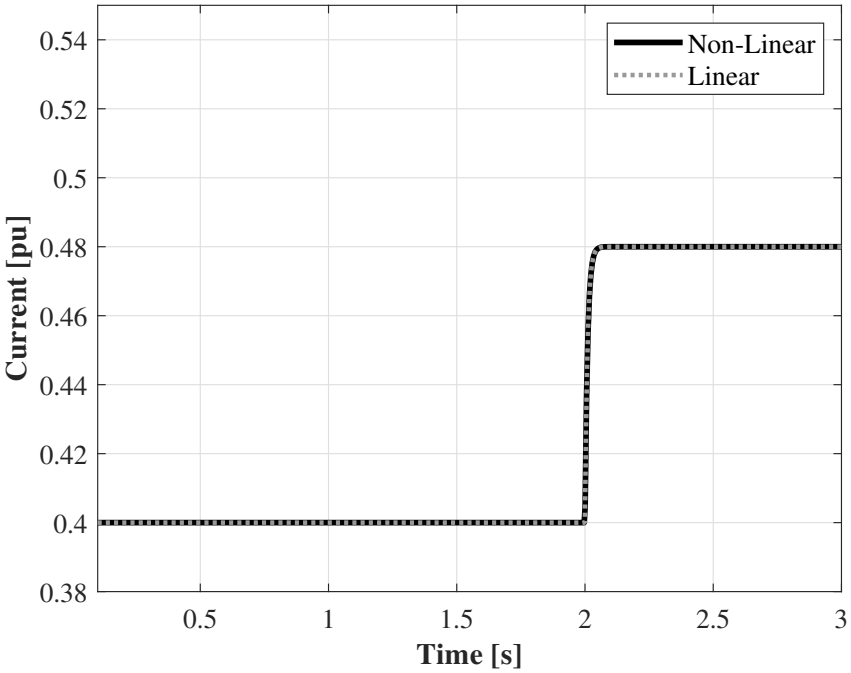


Figure 44: Small perturbation in the current $i^c_{f\_q}$ of the converter

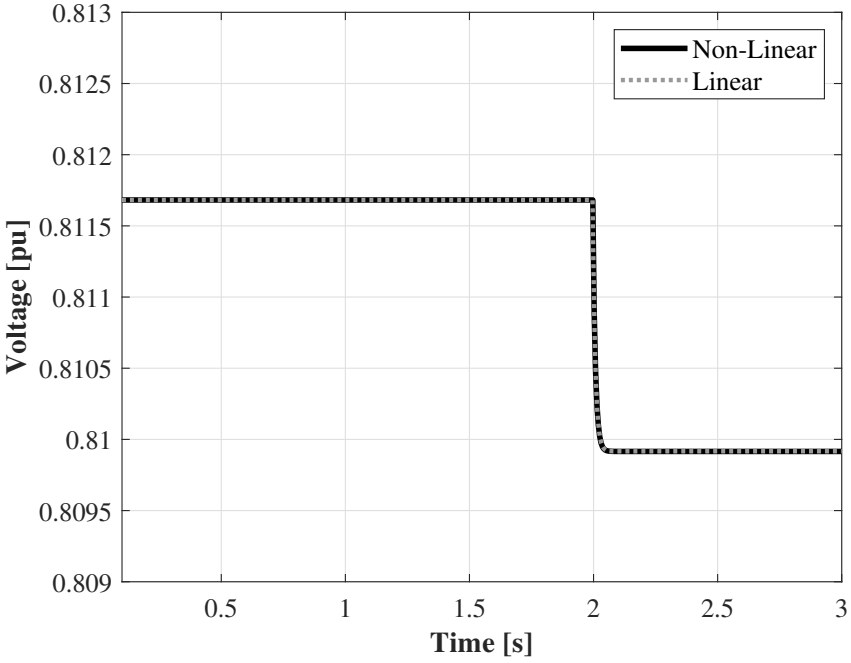


Figure 45: Small perturbation in the PCC voltage $V^c_{pcc\_q}$

Fig. 46, Fig. 47, Fig. 48 shows the validation of the VSC converter connected to the five bus network and equivalent network.

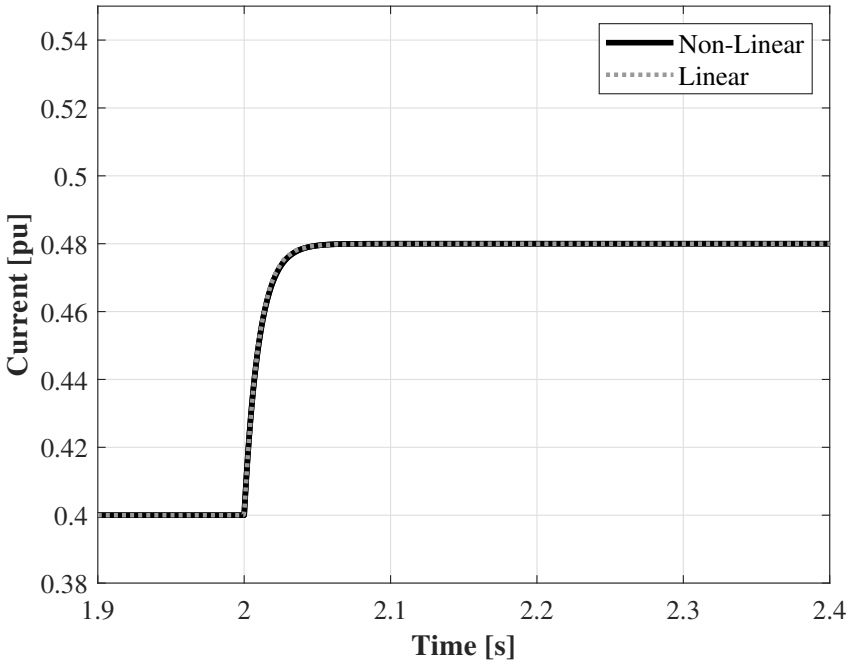


Figure 46: Small perturbation in the current $i^c_{f\_q}$ of the converter

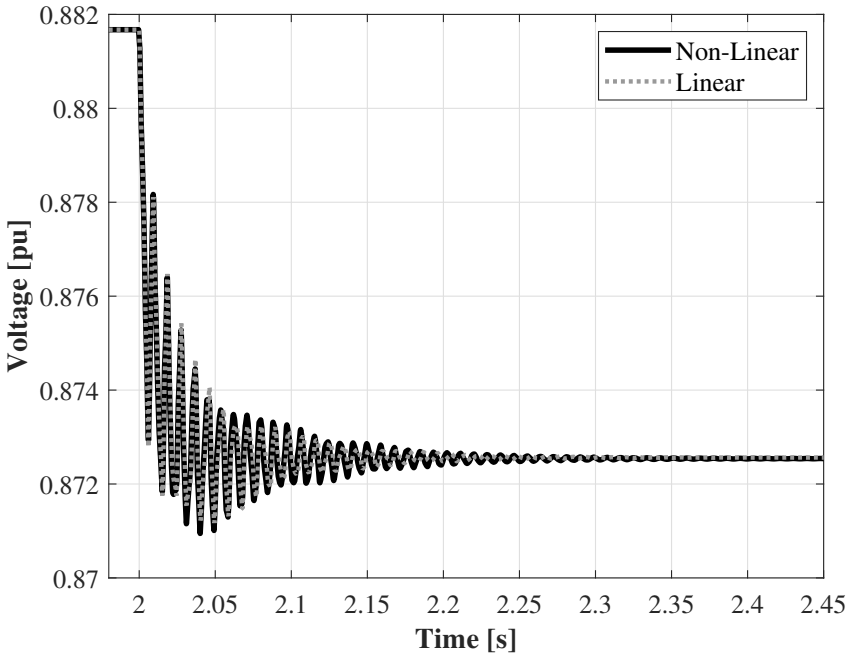


Figure 47: Small perturbation in the PCC voltage $V^c_{pcc\_q}$

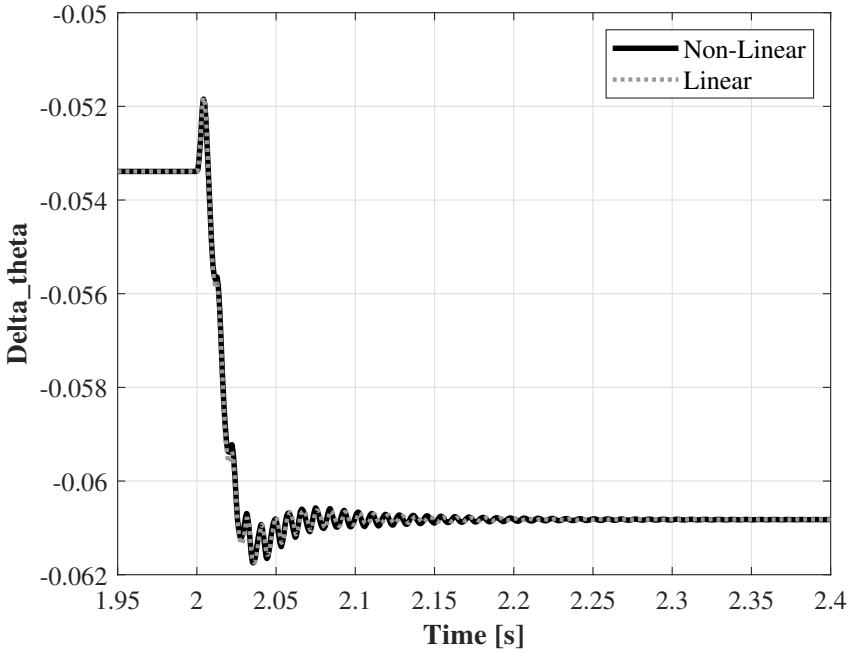


Figure 48: Difference between the estimated angle $\hat{\theta}$ and the grid angle $\theta_g$

## 7.10 Example

In Table 6, it can be observed that there are three poles located in the RHP. Notice that the damping of such poles is negative. The mode number associated to these poles is 21,19 and 20. Looking for those numbers in Fig. 49, it can be seen that the variable $\theta$ (which is a state of the PLL) has the highest participation on those poles. Therefore, it can be said that the PLL is the cause of instability when the system operates at the given conditions of active and reactive power.

Table 6: Modal Parameters

| Mode | Real | Imaginary | Damping | $f_p$ | $f_n$ | $f_r$ |
|---|---|---|---|---|---|---|
| 21 | 171.0870 | 0.0000 | -1.0000 | 0.0000 | 27.2293 | j27.2293 |
| 19 | 55.2985 | 422.1217 | -0.1299 | 67.1828 | 67.7568 | 66.6038 |
| 20 | 55.2985 | -422.1217 | -0.1299 | 67.1828 | 67.7568 | 66.6038 |
| 1 | -19.2505 | 4167.0381 | 0.0046 | 663.2047 | 663.2118 | 663.1976 |
| 2 | -19.2505 | -4167.0381 | 0.0046 | 663.2047 | 663.2118 | 663.1976 |
| 3 | -18.5547 | 3465.8709 | 0.0054 | 551.6105 | 551.6184 | 551.6026 |
| 4 | -18.5547 | -3465.8709 | 0.0054 | 551.6105 | 551.6184 | 551.6026 |
| 5 | -19.2296 | 3538.7818 | 0.0054 | 563.2146 | 563.2229 | 563.2063 |
| 6 | -19.2296 | -3538.7818 | 0.0054 | 563.2146 | 563.2229 | 563.2063 |
| 7 | -17.3164 | 2840.6156 | 0.0061 | 452.0980 | 452.1064 | 452.0896 |
| 8 | -17.3164 | -2840.6156 | 0.0061 | 452.0980 | 452.1064 | 452.0896 |
| 9 | -19.1459 | 2754.3162 | 0.0070 | 438.3630 | 438.3736 | 438.3525 |
| 10 | -19.1459 | -2754.3162 | 0.0070 | 438.3630 | 438.3736 | 438.3525 |
| 17 | -7.2062 | 1006.5308 | 0.0072 | 160.1943 | 160.1985 | 160.1902 |
| 18 | -7.2062 | -1006.5308 | 0.0072 | 160.1943 | 160.1985 | 160.1902 |
| 13 | -18.6809 | 2126.8789 | 0.0088 | 338.5033 | 338.5163 | 338.4902 |
| 14 | -18.6809 | -2126.8789 | 0.0088 | 338.5033 | 338.5163 | 338.4902 |
| 11 | -20.3518 | 2239.6444 | 0.0091 | 356.4505 | 356.4652 | 356.4358 |
| 12 | -20.3518 | -2239.6444 | 0.0091 | 356.4505 | 356.4652 | 356.4358 |
| 15 | -20.1637 | 1611.6022 | 0.0125 | 256.4945 | 256.5145 | 256.4744 |
| 16 | -20.1637 | -1611.6022 | 0.0125 | 256.4945 | 256.5145 | 256.4744 |
| 25 | -41.0156 | 314.1593 | 0.1295 | 50.0000 | 50.4243 | 49.5720 |
| 26 | -41.0156 | -314.1593 | 0.1295 | 50.0000 | 50.4243 | 49.5720 |
| 23 | -41.0681 | 314.1593 | 0.1296 | 50.0000 | 50.4254 | 49.5709 |
| 24 | -41.0681 | -314.1593 | 0.1296 | 50.0000 | 50.4254 | 49.5709 |
| 22 | -204.5919 | 0.0000 | 1.0000 | 0.0000 | 32.5618 | 0.0000 |
| 27 | -76.8364 | 0.0000 | 1.0000 | 0.0000 | 12.2289 | 0.0000 |
| 28 | -1.0645 | 0.0000 | 1.0000 | 0.0000 | 0.1694 | 0.0000 |
| 29 | -100.0000 | 0.0000 | 1.0000 | 0.0000 | 15.9155 | 0.0000 |
| 30 | -3.2117 | 0.0000 | 1.0000 | 0.0000 | 0.5112 | 0.0000 |

$f_n$= Natural frequency
$f_p$= Poles frequency
$f_r$= Resonance frequency

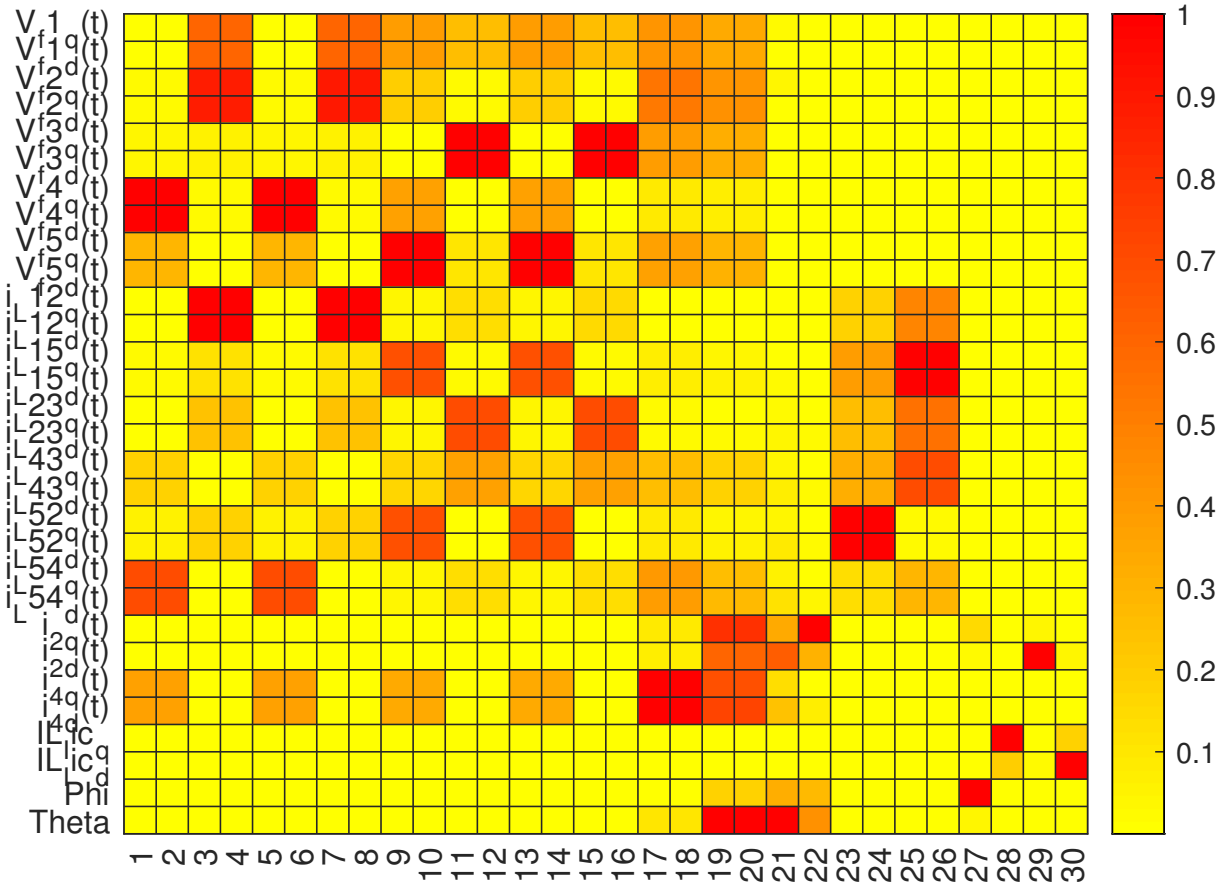


Figure 49: Participation factors

## 7.11 More on power line outage

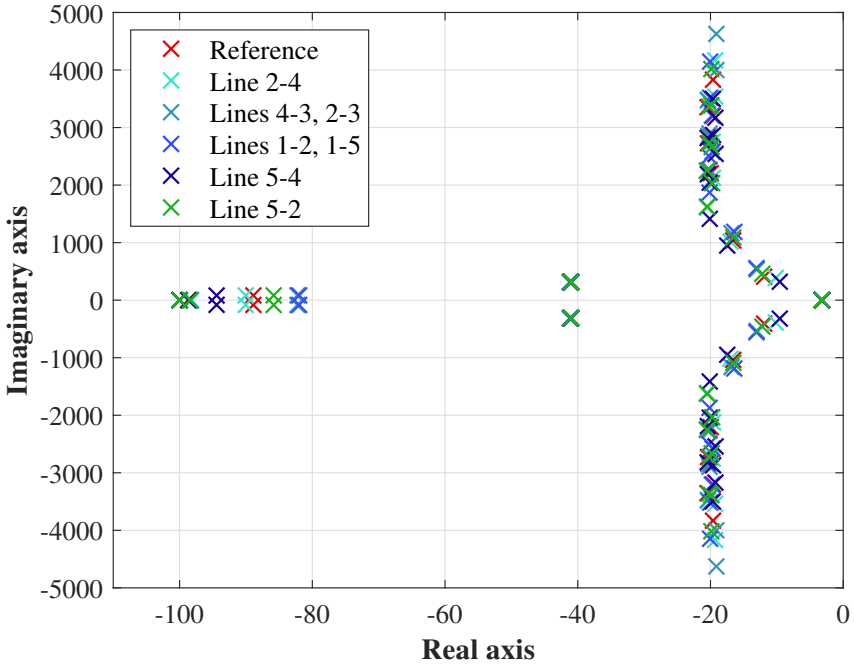


Figure 50: Eigenvalues for the power lines disconnection

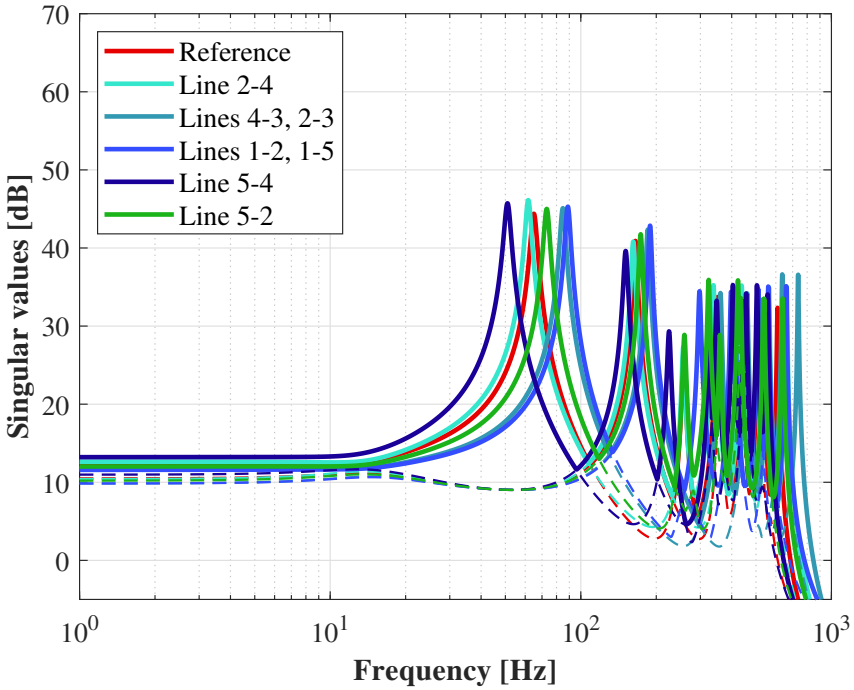


Figure 51: Singular values for the power lines disconnection

## 7.12 Environmental Impact

This project does not have any impact on the environment considering that it is a theoretical project and will not be developed in reality. However, one can consider the environmental impact of the resources used for the development of this thesis.

Consider that this thesis took seven month to be fully completed, working every day an average of 8 hours and 20 days per month. The electrical energy consumed by the computer and lighting of the office should be considered and it is shown in the following table:

| Consumer | Quantity | Power (W) | Usage per month (h) | Months | Energy (kWh) |
|---|---|---|---|---|---|
| Lamps | 9 | 36 | 160 | 7 | 363 |
| Computer | 1 | 50 | 160 | 7 | 56 |
| Total | | | | | 419 |

According to [32], the Spanish electricity mix in 2017 on average produced 0.28 $\mathrm{kgCO_2/kWh}$. Therefore, the impact of the electricity consumption is of $419 \times 0.28 = 117\,\mathrm{kgCO_2}$.

Another thing to consider is the impact of the chosen transport system to move from home to the university, which is at a distance of 2 km away. The chosen transport system is the tram. Four trips were made on average per day. And according to www.terra.org/calc/ the tram usage per year accounts to 73 $\mathrm{kgCO_2}$. And for seven months (20 days per month) this amount accounts to 29 $\mathrm{kgCO_2}$.

It is concluded that this work contributed with 146 $\mathrm{kgCO_2}$ to the environment.